ADDIS ABABA UNIVERSITY

COLLEGE OF NATURAL SCIENCES

SCHOOL OF EARTH SCIENCES

GRAVITY STUDIES OF THE CRUSTAL STRUCTURES BENEATH THE NORTHERN MAIN ETHIOPIAN RIFT AND THE ADJOINING EASTERN PLATEAU

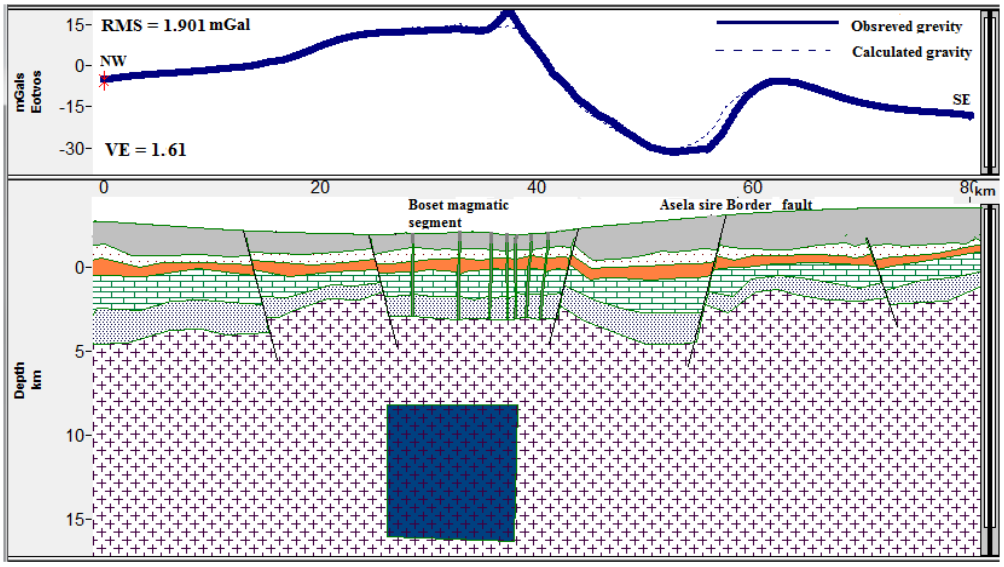

FITHAT HABTEWELD KASSA

A thesis submitted to the school of Graduate studies of Addis Ababa University in partial fulfillment of the requirement for the Degree of Masters of Science in Exploration Geophysics

Submission date

2014

ADDIS ABABA UNIVERSITY

COLLEGE OF NATURAL SCIENCES

SCHOOL OF EARTH SCIENCES

GEOPHYSICAL STUDIES TO MAP CRUSTAL STRUCTURES BENEATH BOTH THE MAGMATIC SEGMENTS IN THE NORTHERN MAIN ETHIOPIAN RIFT AND THE EASTERN BORDER FAULTS

By

Fithat Habteweld Kassa

Approved by board of examiners:

Dr. Seifu Kebede

.....

(Chairman, Department Signature

Graduate Committee)

Dr. Tilahun Mammo

……

Advisor Signature

Dr. Tigstu Haile

……

Internal examiner Signature

Dr. Tesfaye Kidane

……

External examiner Signature

Dr. Mulugeta Alene

……

Chairman Signature

Acknowledgements

My profound gratitude goes to my advisor Dr Tilahun Mammo, for the proper supervision, support and guidance he provided me throughout my research. His critical comments, fatherly approach and unreserved effort have given me the opportunity to explore more.

Special thanks to Geological Survey of Ethiopia for giving relevant data to this work.

At last I would like to express my deepest heart felt gratitude to my family. Their care and encouragement has played important role throughout my academic life.

Table of contents

Page

List of Figures

List of Tables

Acronyms

AS	Analytic Signal
CBA	Complete Bouger Anomaly
EAGLE	Ethiopia Afar Geoscientific Lithospheric Experiment
EARS	East African Rift system
ERS	Ethiopian Rift System
GPS	Global Positioning System
GRS	Geodetic Reference System
IGSN	International Gravity Standardization Network
IUGG	International Union of Geodesy and Geophysics
MER	Main Ethiopian Rift
NMER	Northern Main Ethiopian Rift
RMS	Root Mean Square
SBA	Simple Bouger Anomaly
SER	Southern Ethiopian Rift
SI	Structural Index
TA	Tilt Angle / Tilt Derivative
THDR	Total Horizontal Derivative
VD	Vertical Derivative
V_P	Compressional wave (P-wave) velocity
V_S	Shear Wave (S-wave) velocity
WFB	Wonji Fault Belt
2.5D	Two and Half Dimensional
3D	Three Dimensional

Abstract

The Main Ethiopian Rift (MER) constitutes the northern most part of the East African Rift System (EARS), connecting the EARS with the Afar triple junction and is an area characterised by active extensional tectonics and associated volcanic activities. Structurally the area is generally characterised by intense quaternary faulting and fracturing.

This geophysical investigation comprises of the gravity method of prospecting, carried out in the Northern Main Ethiopian Rift. The method implemented is useful in locating dense intrusion and rift structures like horst and graben. The total gravity data employed in this study were 1230 observation points.The magmatic NMER is believed to represent the transitional stage from continental to oceanic crust. This is due to oceanic crust is denser than that of continental crust. The crust along the NMER shows such kinds of charactersics. The result are presented qualitative and quantitatively in the form of anomaly plots and modeled sections respectively to outline the magmatic segments and the structure beneath them.

The resulting Bouguer gravity map is seen to be dominated by a regional gravity anomaly that increases in amplitude from SW to NE direction of the study area. This increment in Bouguer anomaly value might be due to crustal thining towards in the southern Afar. While the residual gravity anomaly shows shallow features and indicates gravity maxima over the volcanic centers that occur within the study area. The quantitative interpretation is based on 2.5D modeling technique, which is constrained with seismic refraction result and stratigraphy of the area. The result reveals a possible subsurface crustal structures and density distribution beneath the rift. The gravity maxima occurring over the magmatic segments were modeled as dense bodies caused by intrusion into the upper crust. The resulting model suggest that beneath the profiles magma emplacement into the upper crust (or magmatic segment) exist in the form of 15 – 18 km wide with a top at 8 km depth extending to 16 km at the Precambrian basement. The magmatic segements are formed when a magma comes from the upper mantle intrude faults and fractures along the centeral rift. These intrusive igneous bodies are mafic or gabbro in composition and has a possible density values of 2.8 – 3 g/cc.

CHAPTER ONE

INTRODUCTION

1.1 General Overview

The Ethiopian Rift System (ERS) (Fig 1.1) is part of the East African Rift System (EARS) formed by extensional tectonics (Mohr, 1967; Kazmin and Habitemichael Berhe, 1978) and comprises a series of rift zones extending from the Afar triple junction at the Red Sea and Gulf of Aden intersection to the Kenya rift. Rifting in this part of the world started during the early Tertiary period jointly with regional crustal uplift forming the Afro-Arabian dome until the end of the Eocene.

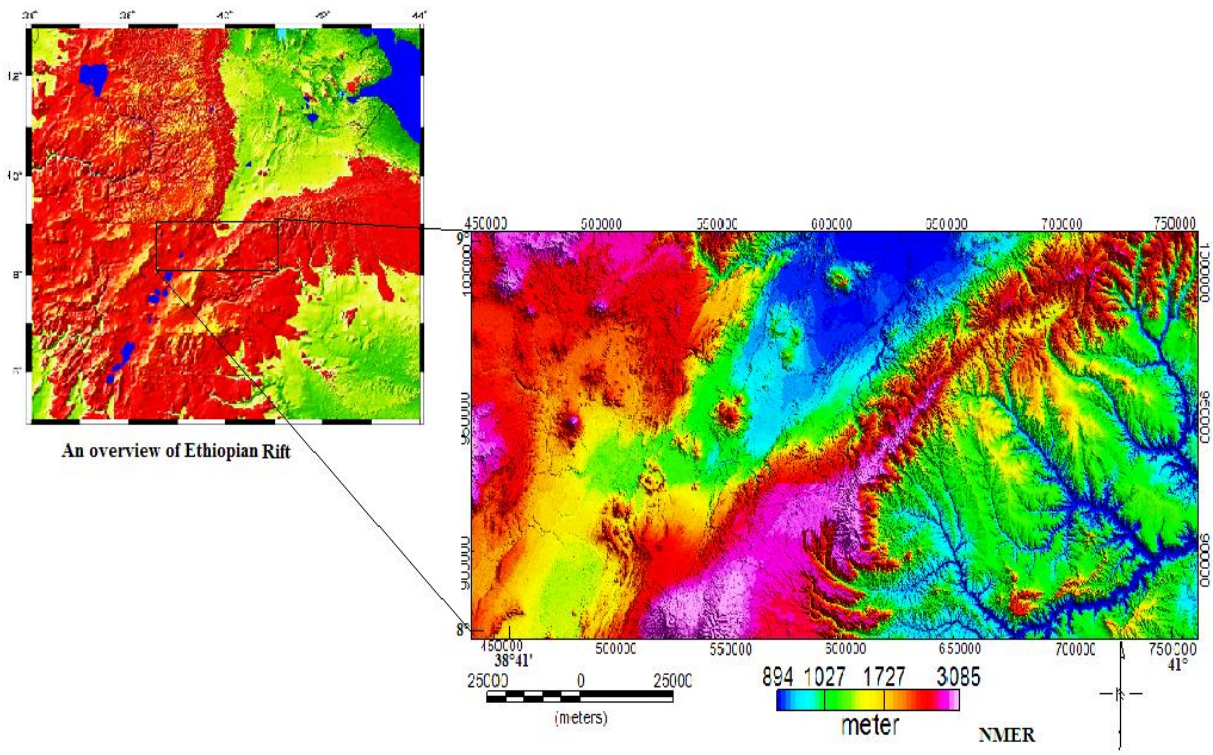

Figure 1.1 An overview of Ethiopian Rift and NMER

The Main Ethiopian Rift (MER) lying within 5°00’ and 11°00’N latitude and 37°00’ and 42°00’ E longitude is the northern most part of the East African Rift System (EARS), connecting the EARS with the Afar Triple Junction and is an area characterized by active

extensional tectonics and volcanism, (Mohr, 1967). The Main Ethiopian Rift is geographically divided in to three sub sectors; northern, central and southern sectors (WoldeGabriel et al., 1990) and it's width increases from the southern (30 – 60 km) to the central (65 – 90 km) and the northern (80 – 120 km) sectors, and is more than 200km wide in the southern part of the Afar rift and is bordered by the Ethiopian plateau to the west and Somalia plateau to the east.

The Main Ethiopian Rift, like the rest of the EARS, has undergone a very complicated geological evolution and tectonic history. Its geometry is characterized by normal step faults and well – developed Quaternary faulting that is mostly related to the Wonji Fault Belt (WFB) with orientation ranging from NNE – SSW to NE – SW (Mohr, 1967; Meyer et al., 1975; Boccaletti et al., 1998; Acocella et al., 2003). The rift valley as a whole was the site of extensive volcanic activities during the Tertiary.

During Pliocene and Quaternary, the MER progressively deepened, evolving through a sequence of interacting half- graben segments marking the boundary between the Nubia and Somalia plates (Hayward and Ebinger, 1996). The MER is limited by discontinuous boundary faults, active from Miocene (Wolde Gabriel et al., 1990). In the MER two main distinct fault systems are recognizable: the older includes a NNE – SSW and NE – SW trending steep, segmented Miocene rift bounding border fault system which is well developed especially along the Eastern margin separating the rift zone from the Somalia plateau. The younger includes Quaternary N – S and NNE – SSW trending right stepping en echelon fault system, which is considered as the axial zone, the youngest part of the rift that presently coincides with the Wonji Fault Belt (WFB). The WFB is located between the rift borders and affects the rift floor branching off from the eastern border. Despite the overall NE – SW trend of the MER, the WFB is characterized by active NNE – SSW trending extension fractures and normal faults, which in many places are associated with fissural and central volcanic activity (Gibson, 1969; Mohr, 1987; Chorowicz et al., 1994; Korme et al., 1997). The normal faults are in most cases arranged in a right stepping en echelon configuration (Mohr, 1968; Boccaletti et al., 1998) and the vertical throws are in the order of several tens of meters (in the axial zone; Gibson, 1969) to several hundreds of meters (in the margins; Hayward and Ebinger, 1996).

Magmatic construction, diking, and faulting during the past 1.6 Ma have created ~20 km wide, ~60-km long magmatic segments with or without axial valleys. Magmatic segments are arranged en echelon within that ~100 km wide rift valley bounded by mid-Miocene border faults (Ebinger and Casey, 2001). Geodetic data show that magmatic segments accommodate 80% of the strain across the rift, indicating that border faults are no longer the locus of extension (Ebinger and Casey, 2001; Corti, 2009). Comparison with mid ocean ridges suggests that magmatic segments, rather than detachment faults, mark the ocean-continent boundary in rifts with a ready magma supply (Ebinger and Casey, 2001). A magma chamber feeds dikes that propagate laterally to form a magmatic segment. The dike intrusion is driven by magma overpressure and tectonic extensional stress. The tectonic stress results in the dikes being oriented perpendicular to the regional extensional stress, and oblique to the older border faults. Dikes commonly are exposed by faults, and indicate an extension direction of 90°–100° (Bonini et al., 1997; Boccaletti et al., 1998). Average lengths of magmatic segments are ~60 km in the Main Ethiopian Rift (Speight et al., 1982).

Previous studies (Ebinger and Casey, 2001) on MER showed that, there are many Quaternary magmatic segments arranged in right stepping en echelon fashion some of which are Koka, Boset and Fentale. Volcanism in the magmatic segments commenced about 1.6 Ma. Most flows emanated from fissures and small cinder cones (WoldeGabriel et al., 1990; Boccaletti et al., 1999). Quaternary basaltic volcanism in the MER is mainly concentrated along the orientation of faults and fractures of the WFB. These eruptions are controlled by extension fractures with chains of scoria cones developed along the fractures.

1.2 Location of the study area

This study mainly focuses on the Northern sector of the Main Ethiopian Rift (NMER) as shown in the Fig 1.2. The study covers wide area lies within the geographic coordinates of 8° - 9° North and 38° 35’ - 41° 12’ East latitude and longitude respectively.

1.3 Statement of the problem

In the past geological and geophysical investigations have been carried out to map magmatic segments, and understand the crust / upper mantle structures beneath the MER.

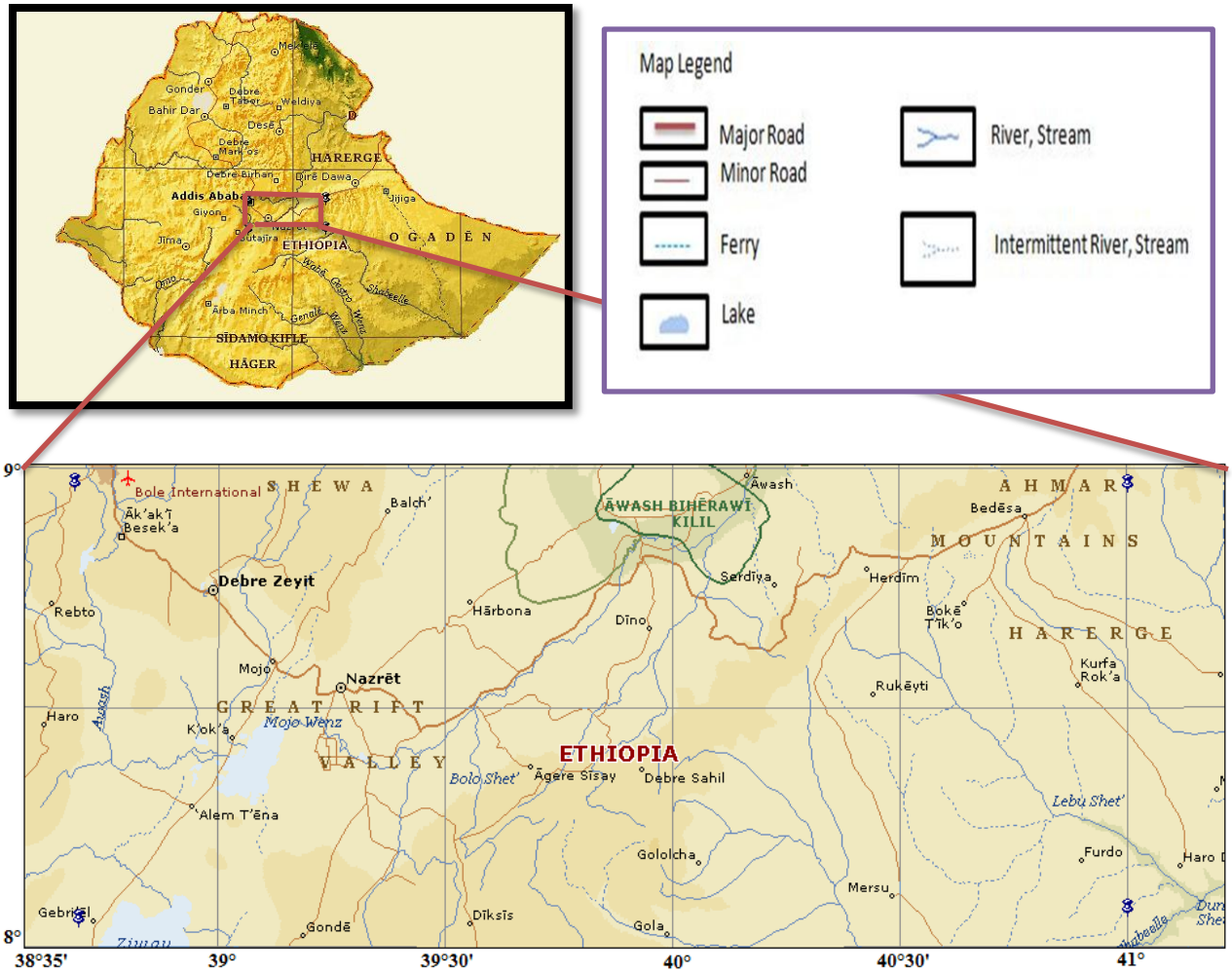

Figure 1.2 Location map of the study area

However, further investigations will be needed to understand the mechanism of the rifting and to what extent the magmatic componenet played a role in the extension process. This thesis uses gravity data to outline the areal and depth extent of the magmatic segments and the border faults in the hope of increasing knowledge in the rifting process.

1.4 Significance of the study

geologically and geophysically the Ethiopian Rift System (ERS) is one of the most interesting studying area in the world. Quaternary faults and volcanic centers define a number of right-stepping en echelon magmatic segments in the Main Ethiopian Rift. Quaternary faults within magmatic segments show predominantly normal slip faults and have eruptive centers or extrusive lavas along their length (Casey et al., 2006). Studying these magmatic segments will provide very important evidence on understanding of rift

extensions. The result of this study also gives better information on subsurface crustal structure in the Main Ethiopian Rift.

1.5 Objectives of the study

1.5.1General objective:

The main objective of this study were gravity studies of the crustal structures beneath the Northern Main Ethiopian Rift and the adjoining Eastern plateau.

1.5.2 Specific objectives:

- To determine depth to the metamorphic basement and depth to the crustal thickness.
- To outline the magmatic segments and the border faults from gravity data analysis.
- To determine the general sub surface structure across the Northern Main Ethiopian Rift.

1.6 Methodology

Geophysical investigation has been used to map crustal structure beneath the magmatic segment and Eastern border fault. The data was collected by CG-3 gravimeter. In order to achieve the objectives of the study different filtering techniques and data reduction process were employed to the raw data gravimeter reading. The gravitational field of the earth is not uniform on the surface of the earth, thus the interpretation of gravity anomaly using a subsurface density variation is complicated by the fact that the variation in the gravitational field of the earth and other factors such as latitude, elevation, terrain (local topography), and instrumental drift & tides.Thus, it is necessary to make corrections to the raw data gravimeter readings to obtain the gravity anomalies that are the target of this study by using different software's. After removing the above effects the interpretation process is complicated by the fact that the reduced gravity data is still the superposition of the effect of the different subsurface density variations. To minimize this effects and to fulfill the above objectives previous geophysical and geological studies have been used in the area of investigation.

The flow chart of the general methodologies that were implemented is given in Figure 1.3.

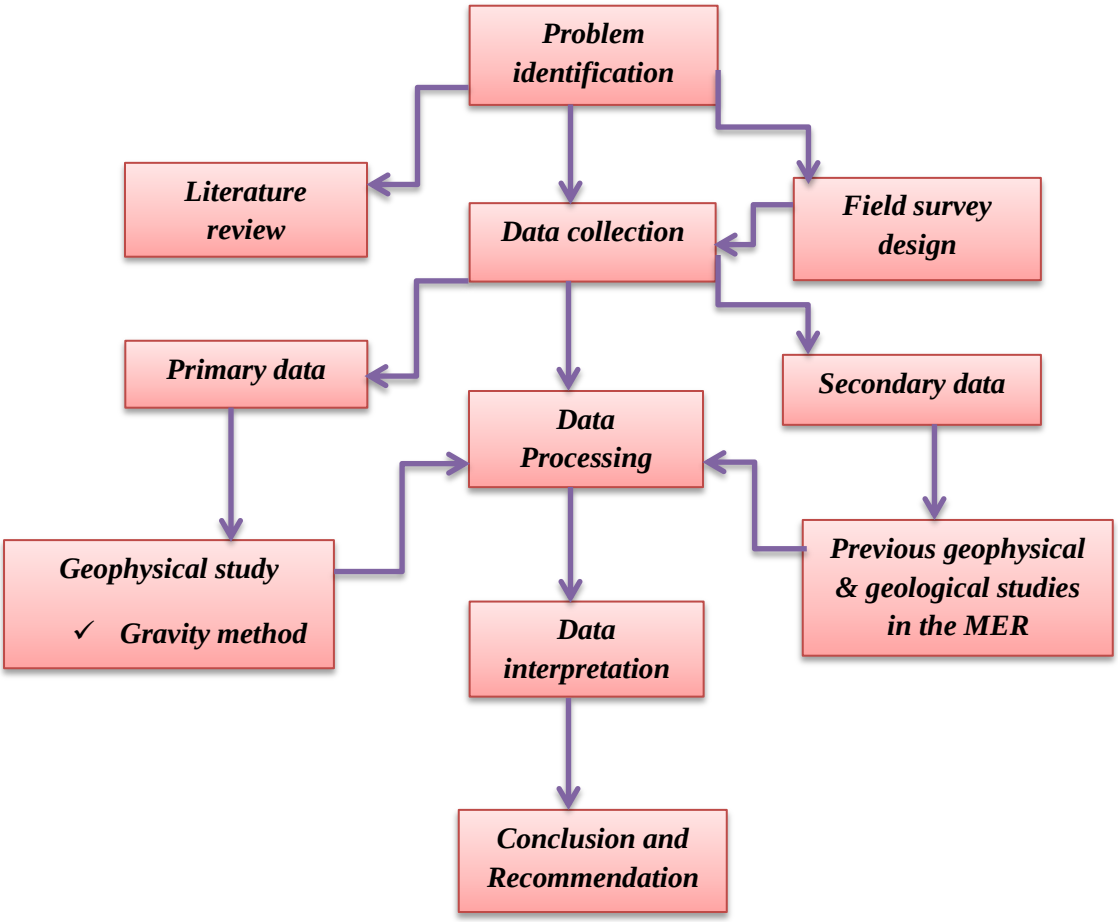

Figure 1.3 Flow chart of the methodology

1.7 Structure of the Thesis

This thesis is organized in to six chapters. The first chapter is general introduction of the study. The second chapter discusses previous geological and geophysical works of the MER as well as the study area. The third chapter addresses the theoretical background of the geophysical method employed in this study. The fourth chapter explains the data acquisition and reduction process. The fifth chapter describes about the qualitative and quantitative interpretation of the maps and models presented. The sixth chapter deals with discussion, conclusion and recommendations of the work. Lastly reference materials used for this work are listed alphabetically.

CHAPTER TWO

GEOLOGICAL AND TECTONIC SETTING

2.1 Geological and tectonic setting of the Main Ethiopian Rift

There is no universal agreement as to when the Ethiopian rift system begins to develop. Different Authors have given different dates (Backer et al., 1972, Meyer et al., 1975, Kazmin, 1979, Kazmin et al., 1980). Burke and Dewey (1970) relate the development of east African rift system to the Afro-Arabian doming in the lower tertiary time. On the other hand Mohr (1967) described the Afro-Arabian rift system is an expression of a tectonic zone of weakness in the lithosphere, which dates back to Precambrian. However, the actual development of the rift is agreed to have commenced at the end of the Mesozoic or the beginning of the tertiary.

Following the Mesozoic era there was extensive magmatism and faulting which modified the face of east Africa. Faulting was accompanied by widespread volcanic activity. The wide spread late Eocene uplift in the Ethio-Arabian region, indicated by rapid marine regression, which is considered to be the formation of the eastern rift system uplift and axial down-wrapping. In Ethiopia these phases where preceded and accompanied by outpouring of the Eocene–Oligocene trap series fissure basalts. Mohr (1971b) recognized three main episodes of swell uplift in Ethiopia; in the late Eocene, middle Miocene, and late Pliocene-early Pleistocene. Trap volcanism in Ethiopia was related to the earliest stage of the uplift.

The opening of the Ethiopian rift is related to the uprising of at least two mantle plumes, presently located beneath the central Gregory Rift in Kenya and beneath the Afar depression. The older Kenyan plume gave rise to the Eocene Oligocene magmatism of Southern Ethiopia (Yemane et al, 1999), which successively migrated southward as a consequence of northward movements of the African plate. The Afar plume is believed to be younger and responsible for the bulk of the magmatism in the central Ethiopia and Afar region (Morley, 1999). From Oligocene to the earliest Miocene following the uplift of the

Afro-Arabian dome, basaltic magma eruptions occurred through fissures in tensional zones (Mohr, 1962a, and 1971b). The rift faulting following the capacious trap volcanics split the crust in to three distinct segments: the Arabian plate, the African plate and the Somalian plate (Mohr, 1971b).

Volcano–tectonic activities during the Cenozoic had played significant roles for the development of the present day Ethiopian rift system. The Ethiopian rift system is part of great East African rift system, widely believed to have been formed by diverging lithospheric plates, which is active since the early tertiary times. The Ethiopian Rift system is commonly used to designate the three discreet rift segments namely, the Afar depression, the Main Ethiopian Rift (MER), and the Southern Ethiopian Rift (SER). The Great east African rift itself is part of the Afro-Arabian rift system that extends for about 6500km (Mohr, 1962) from Turkey in the north to Mozambique in the south passing through the Red sea, Eritrea, Ethiopia, Kenya, Tanzania, and Malawi.

The formation of the MER is attributed to extensional tectonics, though the direction of relative motion between blocks (extensional direction) is still controversial. According to Wolde Gabriel et al., (1990) the development of the rift has been episodic rather than continuous, and a two stage rift development is proposed based on structural and stratigraphic relationship from the central sector of the MER. The initial stage was characterized by the development of a series of half grabens along the rift with alternating polarity (in late Oligocene, early Miocene and early Pliocene times).

The rift valley in the MER separates the Ethiopian and Somalian plateaus, made of uplifted basement rocks, and overlying sedimentary sequences and Eocene-Recent flood basalts. The plateaus rise to elevations >2000 m above sea level as shown in the Fig 2.1; north of latitude 9° the highest elevations are attained by the Ethiopian Plateau, whereas south of this latitude the Somalian plateau reaches the lowest elevations. Local increases in the elevation of the rift valley are generally due to volcanic edifices, as in the Northern MER where several volcanoes raise from the flat rift floor.

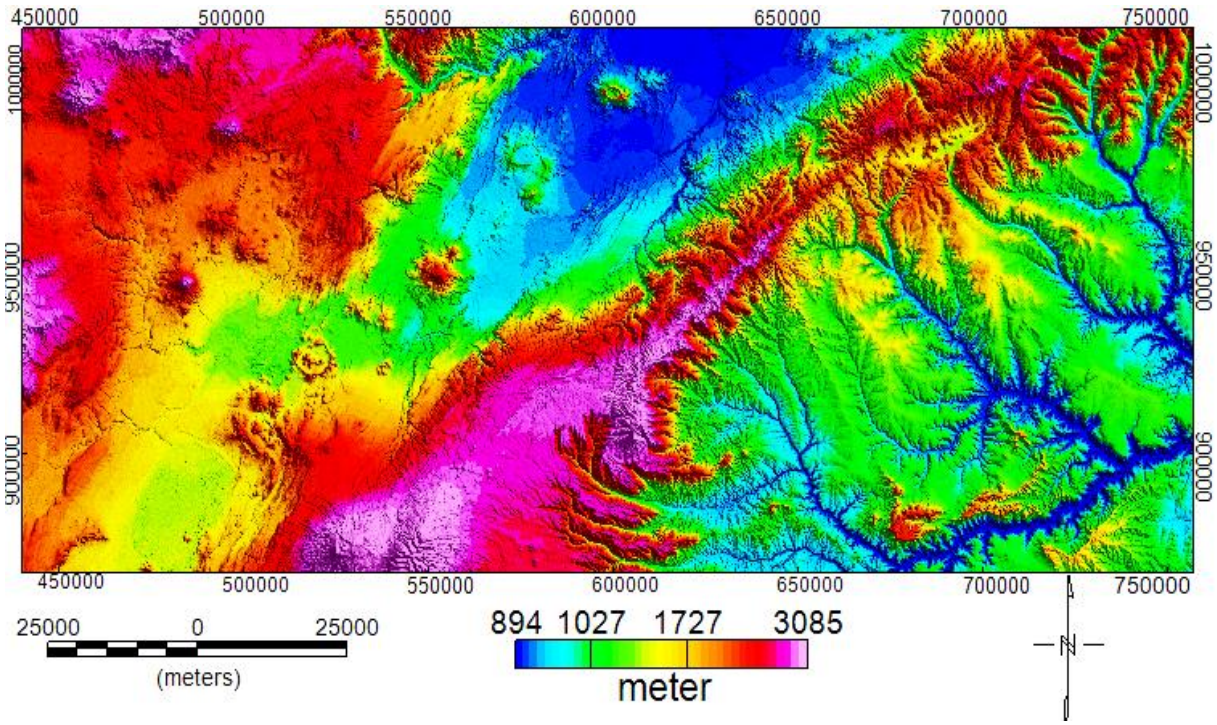

Figure 2.1 Digital elevation model of the study area

The Main Ethiopian Rift is a key sector of the East African Rift System that connects the Afar depression, at Red Sea-Gulf of Aden junction, with the Turkana depression and Kenya Rift to the south (Mohr, 1983; Rosendahl, 1987; Braile et al., 1995; Chorowitz, 2005). It is a magmatic rift that records all the different stages of rift evolution from rift initiation to break-up and embryonic oceanic spreading (Ebinger, 2005), marking the incipient boundary between Nubia and Somalia plates. The Main Ethiopian Rift it is thus an ideal place to analyse the evolution of continental extension, the rupture of lithospheric plates and the dynamics by which distributed continental deformation is progressively focused at oceanic spreading centers. The MER can be subdivided into three segments that have been interpreted to reflect different stages of the continental extension process, being characterised by different fault architecture, timing of volcanism and deformation, crustal and lithospheric structure (Hayward and Ebinger, 1996). The Northern MER extends from the MER-Afar boundary southwards to the Lake Koka area, where it is separated from the Central MER by the Boru Toru Structural High (Bonini et al., 2005). To the south, the boundary between Central and Southern MER can be placed at ~7° N latitude, in the Lake Awasa area, where the rift margins rotates from ~NE-SW to ~N-S, in correspondence to

the Goba-Bonga transverse lineament (Bonini et al., 2005).

The MER is described by a great number of faults which produced a total altitude of more than 1500m (Di Paola, 1972) between the top of the plateau and the floor of the rift. The style of faulting within the MER is dominated by NNE trending swarms of en-echelon tensional faults which commonly produce horsts and grabens. All these faults are normal step faults of various dimensions and throws mainly along NNE-SSW and rarely along NE-SW, N-S and NW-SE directions (Mohr, 1967, Di Paola, 1972).The Wonji Fault Belt (WFB) is the youngest structural deformation, largely concentrated within a narrow, 5-12km wide belt of normal faults in the Ethiopian rift valley that is characterized by NNE-SSW oriented fault zone and running through the whole length of the MER. The WFB is forced into en echelon transpositions in order to remain within the rift margin envelop (Mohr et al, 1980). These sites of transpositions are characterized by very recent and closely spaced normal faults, extensional fractures (Chorowicz et al.,1994) and other faults related open structures with significant volumes of fissural basalts related differentiation products of very recent age and even historical.

Most of the recent (Quaternary) volcanic activity in the MER is closely associated with the Wonji faults, as suggested by alignments of caldera structures, cinder cones, volcanic fissures. Geophysical in the Northern MER have shown the presence of magma throughout the lithosphere below the different fault segments, so that the WFB segments represent tectono-magmatic (or magmatic) segments within the central rift valley (Ebinger and Casey, 2001). In the Northern MER, there are four major WFB segments (Gedemsa, Boseti, Kone and Fantale- Dofen); the en echelon segmentation continues northeastward into the southern Afar depression, where these quaternary tectono-magmatic segments are superposed on the older Red Sea and Gulf of Aden rift structures (Hayward and Ebinger 1996; Wolfenden et al., 2004, 2005) and fault systems display complex geometrical characteristics (distribution of deformation, segmentation, linkage, length/displacement relations, etc.; Soliva and Schultz, 2008). The Wonji faults in the Northern MER are oriented ~N20°, forming an angle of ~20° with the roughly N40° trending boundary faults. The Gedemsa, Boseti and Kone WFB segments are axial ridges, whereas the Fantale-Dofen magmatic segment is marked by a graben that lies 550 m below the Boseti and

Kone segments (Ebinger and Casey, 2001; Casey et al., 2006). The dimensions of individual segments range between 40 and 70 km in length and between 10 and 15 km in width; they are separated by areas devoid of magmatism and brittle deformation (Casey et al., 2006; Kurz et al., 2007) where the distances between segments in an E–W direction vary from 2 km (Boseti segment–Kone segment) to 18 km (Gedemsa segment– Boseti segment). As stated above, each segment is composed of small-displacement faults and extensional fractures. The center of each segment is characterised by significant magmatic deformation accommodated by dyking. Wonji faults are primarily driven by magma intrusion into the mid to upper crust, which triggers upward propagation of faulting and dyke intrusion into the brittle upper crust. Dyke induced growth of normal faults and fractures has been observed during a major magmatic rifting episode at a nascent slow spreading ridge in the Afar depression (Rowland et al., 2007; Ebinger et al., 2008).

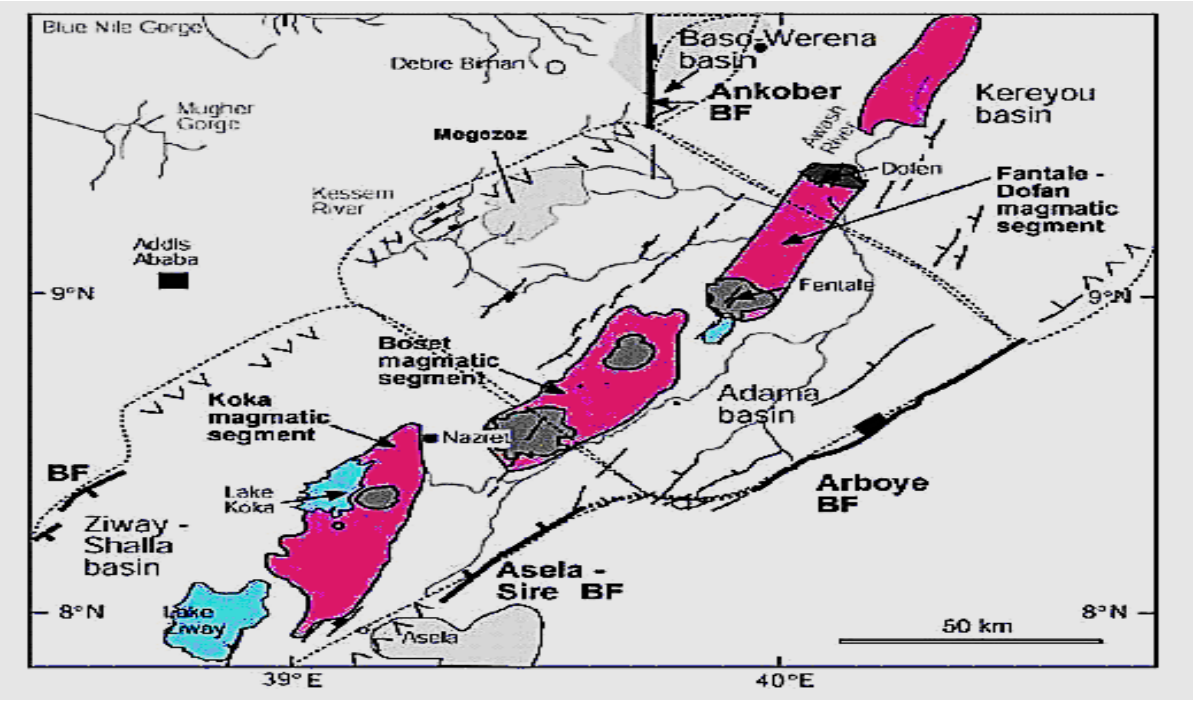

Figure 2.2 Major faults and magmatic segments of the Northern Main Ethiopian Rift (Wolfenden et al, 2004).

The Main Ethiopian Rift is bounded by discontinuous boundary faults that give rise to major fault escarpments as shown in the Fig 2.2 and 2.4 separating the rift depression from the Ethiopian and Somalian plateaus. These faults are normally long, widely spaced and characterised by large vertical offsets >1 km (Boccaletti et al., 1998; Abebe et al., 2007). Their orientation varies in the different rift segments, as illustrated below. In the Northern MER, the boundary faults are oriented ~N40°E. The southeastern basin margin is marked by the major boundary fault systems of Arboye and Sire, which form a staircase pattern rising to the ~2600-m elevation of the uplifted rift flanks (Wolfenden et al., 2004). The Arboye and Sire border fault systems are separated by a right-lateral offset of about 35 km at latitude ~8°20' N; similarly, the Sire fault system dies out to the southwest at latitude ~8°N and is separated by a right-lateral offset of about 15 km from the Asela fault escarpment. Overall, the southwestern margin of this MER sector is characterised by a right stepping en echelon pattern; no major transversal faults are present in these offsets to connect the main fault systems; rather, they are separated by gentle flexure of the Somalian plateau which deeps to the NNE down to the rift depression (Di Paola, 1972; Kazmin et al. 1980). Marginal grabens mark both sides of the Northern MER (WoldeGabriel et al., 2000) although their expression is over printed by younger structures. Field data indicate that the boundary faults of the Northern MER started to develop at around 11 Ma (Wolfenden et al., 2004) geological data and historic and local seismicity patterns indicate these fault systems are largely inactive (Wolfenden et al., 2004; Casey et al., 2006; Keir et al., 2006).

The general succession of the strata in the horn of Africa consists of a Precambrian sequence mainly of metamorphic, Mesozoic sedimentary sequence, Tertiary flood basalts and silicic lava flows with pyroclastic sediments interstratified overlain by Quaternary sediments and alkali silicic lava flows (Mohr, 1971). The rift floor is covered by Mio-Pliocene to present volcanism (basalt, trachytic and rhyolitic lavas, and pyroclastic flows), and volcano sedimentary products (Abate and Saggri, 1980). Most part of the floor of MER is covered by silicic pyroclastic materials, mainly per alkaline rhyolitic ignimbrites, interlayered with basalts and tuffs associated with un-welded pumice (Mohr, 1962, Di Paola, 1972, Weldegebriel et al., 1990) as shown in the Fig 2.3.They are early to middle Pliocene. Alkaline and Per-alkaline rhyolitic lava flows associated with pumice and ash

represent the late silicic volcanic events (Di Paola,1972) where they were erupted from late Pliocene and middle Pleistocene, and in some places outcrop as remnants as large caldera. As summarized by Wolde Gabriel et al., (1990) most of the geological sections exposed along the rift margins are dominated by tertiary volcanic rocks except for a few locations where crystalline basement is unconformabilly overlain by Mesozoic marine sedimentary and/or tertiary volcanic rocks.

2.2. Previous studies in the Main Ethiopian Rift

2.2.1. Crustal structure in the Northern MER

The cross-sectional crustal thickness profile is typical for a continental rift profile, with large border faults bounding the rift, and rift shoulders that are ~5 km thicker than the crust beneath the rift valley (Dugda et al., 2005, 2007; Mackenzie et al., 2005; Maguire et al., 2006; Mickus et al., 2007; Stuart et al., 2006; Keranen et al., 2009) the seismic and structural data show large asymmetries in the basin infill, with tilting towards the large offset border fault system. Along the rift axis, the crust in this rift sector gradually thins to the north, from about 33–35 km at the Northern MER-Central MER boundary to about 24-26 km in southern Afar (Kebede et al., 1996; Dugda et al., 2005; Maguire et al., 2006; Mickus et al., 2007; Stuart et al., 2006). Northward thinning of the crust is mostly accommodated in the upper crust (Mackenzie et al., 2005) the lower crust is instead of rather constant thickness. Locally (as beneath the Fantale–Dofen magmatic segment) the crust is thicker than the surroundings; this is associated with the highest upper-crustal seismic velocity and highest Poisson's ratios, suggesting that magmatic processes may have locally thickened the crust (with respect to the rest of the Northern MER) in a zone of overall extension (Keranen and Klemperer, 2008). Crustal tomography reveals the presence of anomalously fast, elongate bodies in the mid- to lower crust extending along the rift axis and rising to ~10 km subsurface (Keranen et al., 2004; Daly et al., 2008). These 20 km wide and 50 km long bodies are separated and laterally offset from one another in a right-stepping en echelon pattern, approximately mimicking surface segmentation of Quaternary volcanic centers.

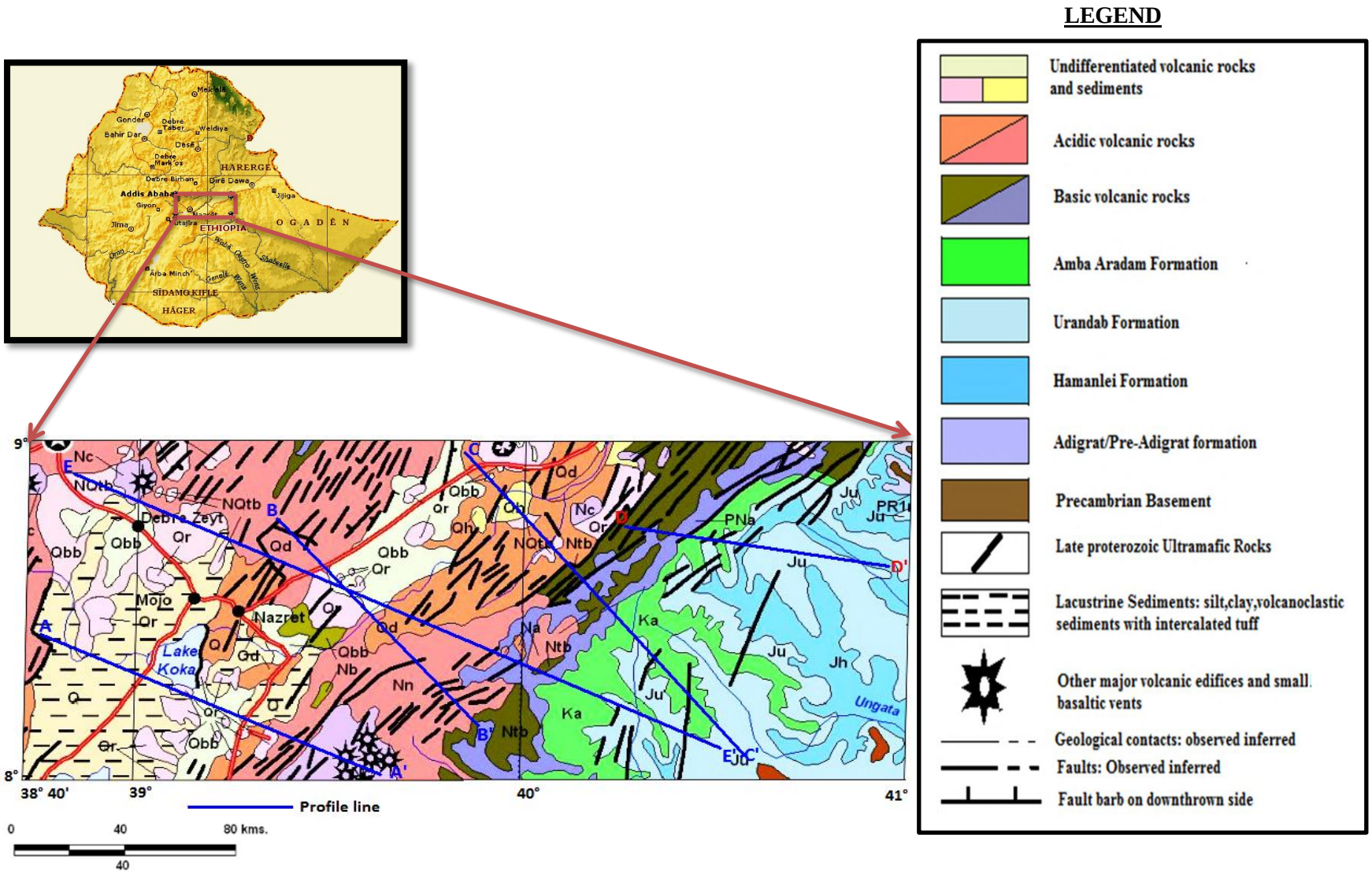

Figure 2.3 Geological map of the study are

The anomalously fast bodies are also characterised by high Vp/Vs ratio (Daly et al., 2008) which increase from beneath the margin of the northwestern plateau into the rift (and northward along the length of the MER; Dugda et al., 2005; Stuart et al., 2006) and by relative positive Bouguer anomalies (Mahatsente et al., 1999, 2000; Tessema and Fontaine, 2004; Tiberi et al., 2005; Cornwell et al., 2006) both features are interpreted as indicating the presence of mid to lower crustal cooled mafic intrusions (Keranen et al., 2004; Daly et al., 2008). Results of gravity analysis by Cornwell et al. (2006) suggest that these intrusions contain at least 40% gabbro. The magnitude of the Vp/Vs ratios and P-wave velocity anomalies along the rift axis could also indicate the presence of a molten fraction in fractures within the solidified mafic intrusions (Dugda et al., 2005; Stuart et al., 2006; Daly et al., 2008) as suggested on the basis of petrological evidences (Rooney et al., 2005).

Figure 2.4 Structural map of the Northern MER (after Casey et al., 2006)

Geophysical data support the presence of melt in the crust and upper mantle beneath Wonji segments. Patterns of seismic velocity anisotropy determined from shear wave splitting studies Kendall et al. (2005 & 2006); Keir et al. (2005) suggest magma intrusion throughout the continental lithosphere beneath Wonji segments. In particular, the magnitude of anisotropy and its parallelism with aligned chains of eruptive centers and fissures suggests the presence of melt-filled cracks and/or dykes that penetrate both the upper crust and the uppermost mantle to a depth of ~75 km (Kendall et al., 2005, 2006; Keir et al., 2005). Similarly, the low lower-crust (and uppermost mantle) shear-wave velocity beneath the rift imaged by Keranen et al. (2009) indicates high temperatures and the presence of melt. Magnetotelluric analysis (Whaler and Hautot, 2006) image a low resistivity zone at ~1 km depth beneath Boseti volcano, which may represent a shallow magma body; presence of magma bodies in the uppermost crust is also supported by gravity modeling (Cornwell et al., 2006). The above findings indicate that the crust beneath the rifted regions in Ethiopia has been extensively modified by magmatic processes and by the addition of mafic rock in the mid to lower crust. Geophysical data support that magmatic modification increases northwards from the Northern MER to the Southern Afar, i.e. towards the more oceanic part of the rift (Kendall et al., 2006) consistent with a northward increase in thinning. Notably, this thinning is mostly accommodated in the upper to middle crust, whereas the lower crust has relatively constant thickness along the length of rift suggestive of a low strength and viscous behavior, possibly caused by high temperatures and presence of melt (Keranen et al., 2009).GPS measurements show that approximately 80% of current extensional deformation across the Northern MER is accommodated in a ~20-km-wide zone of faulting and volcanism within Wonji segments (Bilham et al., 1999).

2.2.2 Seismicity and distribution of current deformation

The MER is characterised by diffuse seismic activity, which is usually represented by small to intermediate size events. Historical records spanning the past 150 years show that large magnitude (M>6) earthquakes are rare throughout the rift (e.g., Gouin, 1979; Asfaw, 1990; Kebede and Kulhánek, 1991; Foster and Jackson, 1998; Ayele and Kulhánek, 2000; Hofstetter and Beyth, 2003; Keir et al., 2006) although seismic analysis suggest a maximal expected magnitude of ~7, with return period of about 80 yr (Horsfetter and Beyth, 2003).

Despite the widespread seismic activity, a comparison of the expected released seismic moment and observed seismic moment for the period 1960–2000 suggests that less than 50% of extension across the MER may be accommodated by rapid slip on faults (Hofstetter and Beyth, 2003). Thus most of the extensional deformation (>50%) seems to be accommodated aseismically. Slip on faults appears to have slowed in favor of dike injection associated with magmatic segments in the past ~1.8 Ma (e.g., Keir et al., 2006) and that a combination of dyking and normal faulting within the Wonji segments appears to be the predominant mechanism of extension in the MER.

Detailed data about the seismicity of the Northern and Central MER have been acquired in the period from October 2001 to January 2003 by the EAGLE network of seismic stations (Keir et al., 2006). These data show that the seismic activity in the Northern and Central MER is typically localised within Wonji segments (Keir et al., 2006) pointing to a close correlation between seismicity and alignments of Quaternary volcano-tectonic zones as shown in the Fig 2.5.

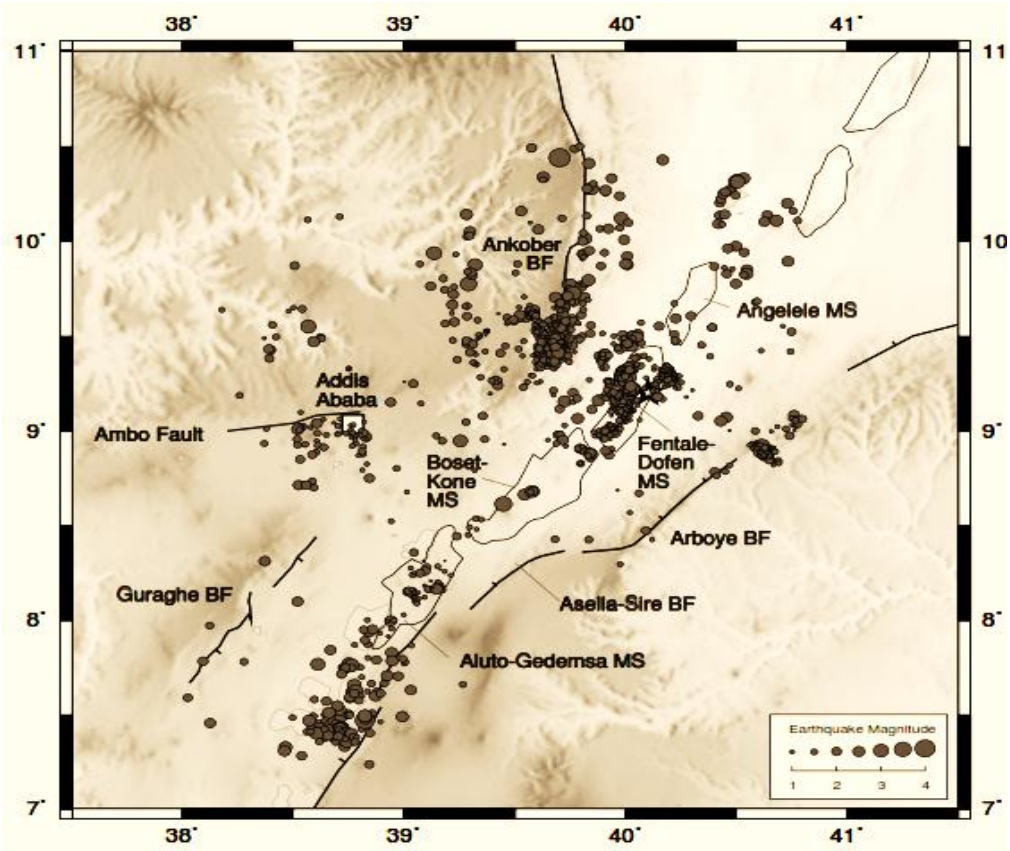

Figure 2.5 Seismicity distribution in the Northern Main Ethiopian Rift (Derek Keir thesis, 2006)

Major boundary faults are largely aseismic, although cluster of events may characterise the border escarpments in structurally complex region that still experiences some strain (as the Arboye border fault system, at the intersection between the north striking Red Sea rift and the NE striking MER (Keir et al., 2006). Historical data support the inactivity of border faults, highlighting the lack of large magnitude earthquakes on these fault systems over the last ~50 years in the Northern and Central MER (Ayele and Kulhánek, 1997). Clusters of earthquakes are located in narrow regions within Wonji segments, with elongation paralleling the surface expression of major Quaternary faults and volcanic fissures (Keir et al., 2006). In the Northern MER, the area affected by seismic events is only 10-km wide; whereas in the Central MER seismicity is comparatively more diffuse than to the north and located within a 30 to 40 km wide zone. The regions connecting the right stepping en echelon WFB zones are largely aseismic. Most earthquake hypocenters are located at a depth of ~8-16 km, which coincides with the top of the middle to lower crustal extensive mafic intrusions; hypocenter depths increase with increasing distance from major volcanoes. The temporal distribution of seismicity in the Fantale-Dofen WFB segment is characterised by earthquake swarms that punctuate largely aseismic periods.

Laser ranging and GPS (geodetical) observations in the rift zone support the seismic observations and indicate that about 80% of the extensional deformation is currently accommodated in correspondence to the narrow regions of seismic activity, along the en-echelon faults of the Wonji fault belt (Bilham et al., 1999).

CHAPTER THREE

GEOPHYSICAL METHOD

3.1 THE GRAVITY METHOD

In exploration geophysics, the gravity method exploits the earth's field difference caused by lateral density variations in the earth's crust. If geologic movements causes in the dislocation of rocks of different densities, the result in lateral density distribution will make corresponding variation in the gravity field. The measured variation in the earth's gravity field is interpreted as convincing subsurface mass distributions. The gravity method is also used in modeling the earth's crust, in locating area of anomalous mantle materials (in areas of plate margins) and it is the basis for the study of the earth's shape (Telford, 1990). The method of gravity surveys in geophysics involves measurement, reduction, mapping, and interpretation of gravity data (Dobrin, 1988). Gravimetry is the method of measuring and modeling the gravity field of the earth (Torge, 1989).

3.1.1 Fundamental Principles

Gravity survey is measurement of the gravitational field at a series of different locations over an area of interest. The objective in exploration work is to associate gravity variations with differences in the density distribution.

The bases of gravity surveys are based on the mutual attraction experienced between two masses as first expressed by Isaac Newton. Newton's law of gravitation states that "the mutual attractive force between two point masses, m_1 and m_2, is inversely proportional to the square of the distance between them". The constant of proportionality is usually specified as ***G*, the universal gravitational constant.**

Thus, the law of gravitation written as shown below where **F** is the force of attraction, $\mathbf{G = 6.67 \times 10^{-11}\ Nm^2/Kg^2}$ is the gravitational constant and **r** is the distance between the two masses, $\mathbf{m_1}$ & $\mathbf{m_2}$ and $\hat{\mathbf{e}}$ is a unit vector whose direction is the line connecting the center of the two masses.

$$F = \frac{Gm_1m_2}{r^2}\,\hat{e} \tag{3.1}$$

When making measurements of the earth's gravity, we usually don't measures the gravitational force, **F** rather; we measure the gravitational acceleration, **g**. The gravitational acceleration is the time rate of change of a body's speed under the influence of the gravitational force.

Newton also defined the relationship between a force and acceleration. Newton's second law states that: force is proportional to acceleration. The constant of proportionality is the mass of the object.

$$F = \frac{Gm_1m_2}{r^2}\,\hat{e} = m_2 g \tag{3.2}$$

For the case of the earth of mass $\mathbf{M_e}$ and a body of mass, **m** located on or in the vicinity of its surface:

$$F = \frac{G\,M_e m}{r^2}\,\hat{e} = mg \tag{3.3}$$

From the above equation (eq.3.3);

$$\vec{g} = \frac{G\,M_e}{r^2}\,\hat{e} \tag{3.4}$$

g – is gravity or acceleration due to gravity. The unit of **'g'** is **Gal** in the honor of **Galileo Galilei 1 Gal = 1cm /s2.** In geophysics we also use auxiliary units like mill Gal **($mGal$)**, micro Gal **(μ Gal**) and so on. But the **mGal** unit commonly used. **1mGal** = **10^{-3}cm/s2.**

3.1.2 Theoretical Gravity of the Earth

Considering a small mass, **m** moving with a velocity **v**, on the surface of the earth rotating with angular velocity **ω** as shown in the Fig 3.1**,** it is possible to develop the theoretical gravity or the normal gravity value of the earth.

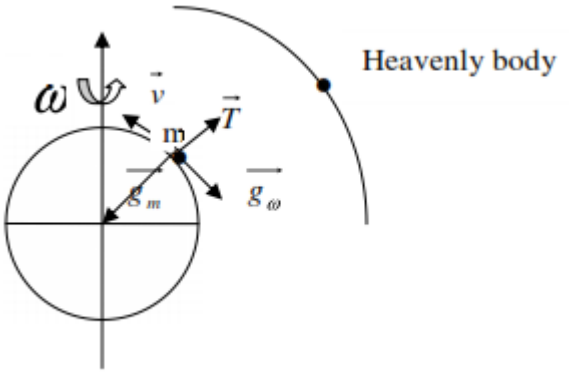

Figure 3.1 Gravity force per unit mass acting on a mass, m on earth

where $\mathbf{g_m}$ - attraction force per unit mass acting on **m** due to earth's mass.

$\mathbf{g_\omega}$ - Centrifugal force per unit mass acting on **m** due to earth's rotation with $\boldsymbol{\omega}$.

T- Tidal force per unit mass acting on **m** due to mass attraction of other heavenly bodies.

The resultant force per unit mass acting on m is;

$$\vec{g} = \overrightarrow{g_m} + \overrightarrow{g_\omega} + \vec{C} + \vec{T} \tag{3.5}$$

where **C** is Coriolis force acting on **m** due to its motion, and its value is zero if **m** is at rest on the earth's surface. If we assume the earth to be spherical in shape with radius R;

$$\overrightarrow{g_m} = \frac{G\,M}{R^2}\,\hat{e} \text{ and } \overrightarrow{g_\omega} = \vec{\omega}\left(\vec{\omega} \times \vec{R}\right) \tag{3.6}$$

The effect of **C** and **T** on $\vec{g}$ is usually considered negligible in actual work. Therefore, gravity $\vec{g}$ refers to the combined effect of both earth mass gravitation and rotation.

$$\vec{g} = \overrightarrow{g_m} + \overrightarrow{g_\omega} \text{ Or } \frac{G\,M}{R^2}\,\hat{e} + \vec{\omega}\left(\vec{\omega} \times \vec{R}\right) \tag{3.7}$$

3.1.3 The Major Forces Acting on a Body on the Earth's Surface

Assume a spherical shape earth rotating with angular velocity, ω and a small mass resting on the earth's surface as shown in the Fig 3.2.

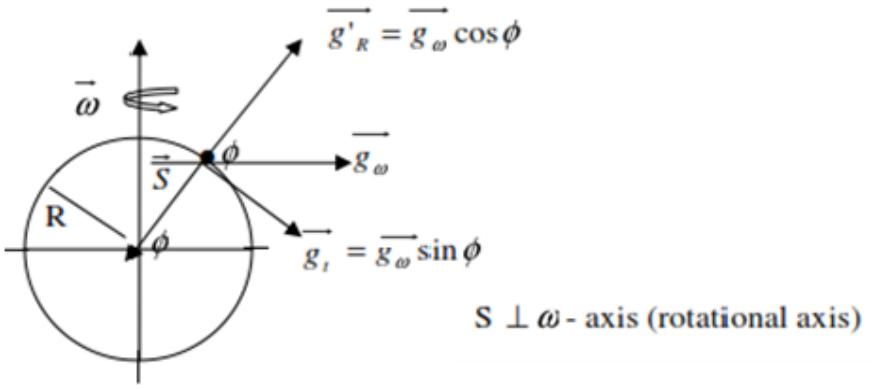

Figure 3.2 components of forces acting on mass, m on earth's surface

From the figure above the force acting on mass **m** placed on the earth's surface are: g_m (attraction force per unit mass due to the earth's mass **M**) and $\mathbf{g}_{\boldsymbol{\omega}}$ (rotational force per unit mass due to the earth's rotation). The resultant gravity force per unit mass on mass **m** will be taken from eq. (3.7).

$$\vec{g} = \overrightarrow{g_m} + \overrightarrow{g_\omega} \tag{3.8}$$

From figure 3.2, the following relations are clearly shown.

$$\vec{S} = R\cos\emptyset \tag{3.9}$$

$$\vec{g}_\omega = \omega^2 S = \omega^2 R\cos\emptyset \tag{3.10}$$

$$\grave{g}_R = \overrightarrow{g_\omega}\cos\emptyset = \omega^2 R\cos^2\emptyset \tag{3.11}$$

$$\grave{g}_t = \overrightarrow{g_\omega}\sin\emptyset = \omega^2 R\sin^2\emptyset \tag{3.12}$$

This implies that;

$$g = g_m - \grave{g}_R = \frac{G M}{R^2} - \omega^2 R\cos^2\emptyset \tag{3.13}$$

where- $\grave{g}_R$' is the radial component of $\vec{g}_\omega$, and

$\grave{g}_t$ is the tangential component $\vec{g}_\omega$. This has no effect on mass m. Therefore; eq. (3.10) will be reduced into:

$$g = \frac{G\,M}{R^2} - \omega^2\, R\cos^2 \emptyset \tag{3.14}$$

- At the equator ($\emptyset = 0^\circ$)

$$g = g_e = \frac{G\,M}{R^2} - \omega^2\, R\cos^2 0^\circ \tag{3.15}$$

$$g_e = \frac{G\,M}{R^2} - \omega^2\, R \tag{3.16}$$

- At the pole ($\emptyset = \pm 90^\circ$)

$$g_p = \frac{G\,M}{R^2} - \omega^2\, R\cos^2 90^\circ \tag{3.17}$$

$$g_p = \frac{G\,M}{R^2} \tag{3.18}$$

From equations (3.16) and (3.18) one can conclude that gravity value **g** is minimum at the equator and maximum at the poles. The real earth observed values of gravity, **g** at the poles and equator are $\mathbf{g_p = 983.218\ Gals}$ and $\mathbf{g_e = 978.032\ Gals}$ respectively. The difference between $\mathbf{g_p}$ **and** $\mathbf{g_e}$ yields about **5.2 Gals** $\mathbf{(g_p - g_e = 5.2\ Gals)}$ and calculations on a theoretical basis for a spherical earth model is about **3.4 Gals** $\mathbf{(g_p - g_e = \omega^2 R = 3.4\ Gals)}$**.** The disagreement between observed values of gravity $\boldsymbol{g}$ for a real earth and calculated value of gravity, **g** for a spherical model earth is due to the assumptions used above. From these disagreements one can conclude that;

- The shape of the real earth is not spherical.
- The shape of the earth is rotationally distorted such that its shape is flattened at the poles and bulged at the equator.
- Gravity value, **g** varies as a function of latitude, ∅.

3.1.4 The Geoids and the Reference Ellipsoid

Geodesist and geophysicists consider two surfaces that represent the average shape of rotationally distorted real earth to study its gravity field, shape and size. These are the geoid and the reference ellipsoid as shown in the Fig 3.3.

A) The Reference Ellipsoid.

An idealized geometrical or mathematically generated theoretical earth model flattened at the poles and bulged at the equator. This model of the earth assumes no undulations on the earth's surface where as we have hills, mountains and depressions on the real earth. It also considers only radial variations in density of the earth plus centrifugal acceleration. A theoretical earth model upon which the variation of gravity, **g** with latitude **(∅)** is computed according to an international agreements in 1967 by IUGG as:

$$\gamma = g_e(1 + C_1 \sin^2 \emptyset + C_2 \sin^2 2\emptyset) \quad (3.19)$$

where $g_e = 978.0490, C_1 = 0.0052884$ and $C_2 = -0.0000059$

B) The Geoid

A physical surface on earth referred to the mean sea level that must be related to the reference ellipsoid for its practical work. The geoid is a practical surface on which **g** values observed on the actual to the topography of the real earth are mathematically shifted to its surface using gravity reduction methods which we are going to discuss later. Unlike the reference ellipsoid, the geoid shows wide undulations following topography of real earth. And also the geoid considers both radial and lateral variation in density of the earth and centrifugal acceleration.

3.1.5 Gravity corrections

The gravity method involves measuring the earth's gravitational field at specific locations on the earth's surface to determine the location of subsurface density variations. These variations in gravitational acceleration of the earth are subdivided into two categories.

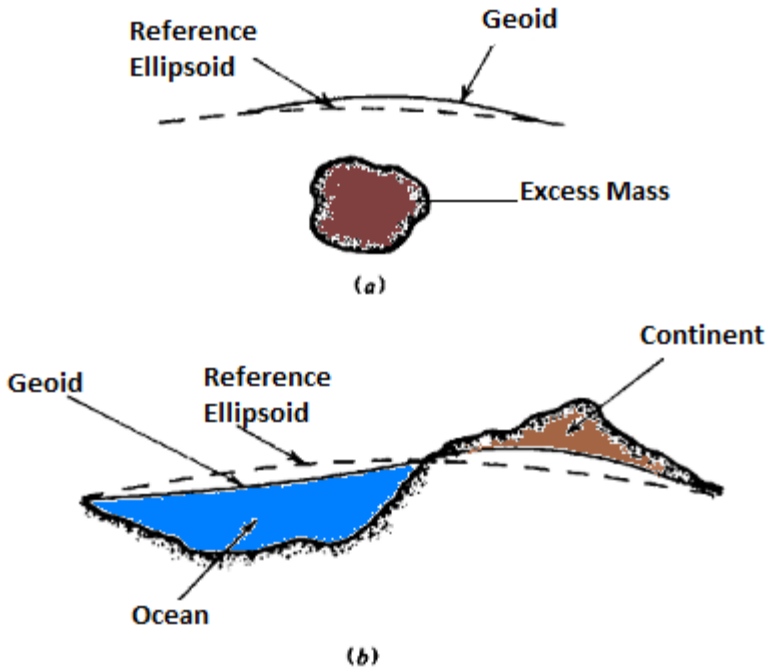

Figure 3.3 Comparison of the reference ellipsoid and geoid (a) The real earth model of topography, geoid and ellipsoid (b)

I Temporal Based Variations - These are changes in the observed acceleration that are time dependent. In other words, these factors cause variations in acceleration that would be observed even if we didn't move our gravimeter.

- ✓ **Instrument Drift** - Changes in the observed acceleration caused by changes in the response of the gravimeter over time.
- ✓ **Tidal Affects** - Changes in the observed acceleration caused by the gravitational attraction of the sun and moon.

II Spatial Based Variations - These are changes in the observed acceleration that are space dependent. That is, these are the change in the gravitational acceleration from place to place.

- ✓ **Latitude Variations** - Changes in the observed acceleration caused by the ellipsoidal shape and the rotation of the earth.
- ✓ **Elevation Variations** - Changes in the observed acceleration caused by differences in the elevations of the observation points.

- ✓ **Slab Effects** - Changes in the observed acceleration caused by the extra mass underlying observation points at higher elevations.
- ✓ **Topographic Effects** - Changes in the observed acceleration related to topography near the observation point.

The gravity $\boldsymbol{g}$ values that we determine by gravity surveying are different from place to place on the actual surface of the earth all over the world. The readings will generally be influenced by latitude, tidal effect and instrumental drift, elevation and topography. To reduce them to the value they would have on some datum equipotential surface such as the geoid, or surface everywhere parallel to it, some adjustment is important. The following are important components of gravity data correction; free air correction, Bouguer correction, Terrain (topographic) correction, latitude correction and drift correction.

Instrument Drift Correction

Drift is a gradual and unintentional change with time as a result of elastic creep in the springs, producing an apparent change in gravity at a given station. These variations in spring properties with time can be due to stretching of the spring over time or to changes in spring properties related to temperature changes. To help minimize the later, gravimeters are either temperature controlled or constructed out of materials that are relatively insensitive to temperature changes. This drift is corrected for by including base station readings in your survey. The base station is a reference station that is kept constant throughout a survey and is revisited ever 1 to 2 hours each day during a survey. These regular base station measurements are used to correct for drift variations. It is assumed that the drift components of the gravity field varies linearly between two base station readings, therefore the time-varying components of the gravity field can be easily predicted, and remove.

Tidal correction

Tidal Effect is the variations in gravity observations resulting from the attraction of the moon & sun and the distortion of the earth so produced. Unlike instrument drifts, which results from the temporally varying characteristics of the gravimeter, tidal effect represents real changes in the gravitational acceleration.

Repeated measurements at the same stations permit estimation of the necessary correction for tidal effects over short intervals, in addition to determination of the instrumental drift for a gravimeter. Unfortunately, these are changes that does not relate to local geology and are hence a form of noise in our observations.

Latitude Correction

Both the rotation of the earth and its slights equatorial bulge produce an increase of gravity with latitude. The centrifugal acceleration due to its spinning earth, maximum at the equator and zero at the poles opposes the gravitational acceleration while polar flattening also increases gravity at the poles (Telford, 1990).this combined effect of the earth produces an increase in the value of g with latitude. Generally g increases from $9.78\ m/s^2$ at the equator to $9.83\ m/s^2$ at the poles. The variation of gravity with latitude over the surface of an ellipsoidal earth can be expressed using the theoretical gravity formula IUGG (1967). The latitude correction dg_L is obtained by differentiating the theoretical gravity formula:

$$\frac{dgL}{ds}=\left(\frac{1}{R}\right)\frac{dg_{\emptyset}}{d\emptyset} = 0.811\ (\sin 2\emptyset) mgal.\ \text{N-S direction} \qquad (3.20)$$

where, R- is the mean radius of the earth

$\emptyset$ - Geographic latitude

$ds = Rd\emptyset$ - is N-S horizontal distance (in Km)

Since gravity increases with latitude (both N and S), the above correction is always added as one goes towards the equator.

Free Air Correction

The free air correction is based on the fact that the attraction of the earth as a whole can be considered to be the same as if its mass were concentrated at its center. Hence, it is necessary to correct the readings so that all the field readings are reduced to a datum surface. The correction factor for free air correction has been calculated as:

$$\delta g_{FA} = 0.3086h\ {}^{\text{mGal}}/_{\text{m}} \qquad (3.21)$$

where, h - is the topographic height above sea level.

Note that the free air correction is added to the gravity readings when the station is above the geoid and subtracted when below it.

Bouguer Correction

The Bouguer correction accounts for attraction of material between the station and the datum plane, which was ignored in the free air calculation. If the station were centrally located on a plateau of large horizontal extent and uniform thickness and density of gravity readings would be increased by the effect of the slab between the station and the datum plane. The Bouguer correction, derived by assuming the slab to be of infinite horizontal extent is given by:

$$\delta g_B = 2\pi\, G\rho h \tag{3.22}$$

where h is the height of the gravity station above the geoid and G is the gravitational constant and ρ is the density of the material for mean crustal density $(\boldsymbol{\rho = 2.67\, {}^{g}/_{cm^3}})$ and h in meters, the Bouguer correction reduces to:

$$\delta g_B = 0.1119\, {}^{\mathrm{mGal}}/_{\mathrm{m}} \tag{3.23}$$

The Bouguer correction is applied in the opposite sense to free air correction. It is subtracted when the station is above the datum plane and vice-versa.

The Bouguer correction is:

- Subtracted if the station is above the datum plane.
- Added if the station is below the datum plane.

Terrain Correction

This correction accounts for surface irregularities in the vicinity of the station that is hills rising above the gravity station and valleys (or lack of material) below it. Both topographic features affect the gravity measurement in the sense, i.e. reducing the readings due to upward attraction by the excess mass of hills or mass deficiency (less attraction) due to valleys. Terrain corrections are, therefore, always positive and always added to the station reading. Terrain correction is done by computing graphically the gravity effects at the

observation point of all hills above the station level and all valleys below it. A systematic methodology for performing this tasks was formalized by Sigmond Hammer in 1939.

The terrain corrections require the use of a chart known as graticule as well as a good quality of topographic maps (~10m contour interval or better) of the survey area. Then the correction is computed by dividing the terrain into vertical columns using concentric circles of different radii drawn at suitable angular intervals. For such arrangement the correction term is given as

$$dg_{TC} = G\rho\emptyset\left[r_2 - r_1 + (r_1{}^2 + Z^2)^{1/2} - (r_2{}^2 + Z^2)^{1/2}\right] (\text{mgal}) \qquad (3.24)$$

where, T is the terrain factor ρ is density r_1 & r_2 is the inner and outer radii of the sector respectively $\emptyset$ is angular interval for sectors, (rad) and z is mean elevation.

CHAPTER FOUR

DATA ACQUISITION AND REDUCTION

4.1 Data acquisition

Subsurface geology can be investigated by means of gravity survey based on measuring the variation in the earth's gravitational field arising from density differences between subsurface rocks. The method is useful in locating dense intrusion, rift structures like faults, graben and horsts.

The gravity survey was conducted using Scintrex (CG3-M Autograv) gravimeter (Fig 4.1). It has a reading accuracy of 0.01mgal. The position (elevation and coordinate) of the survey stations and base stations were determined using differential GPS source & receiver (Fig 4.1) and Garmin 12. The differential GPS has a decimeter accuracy.

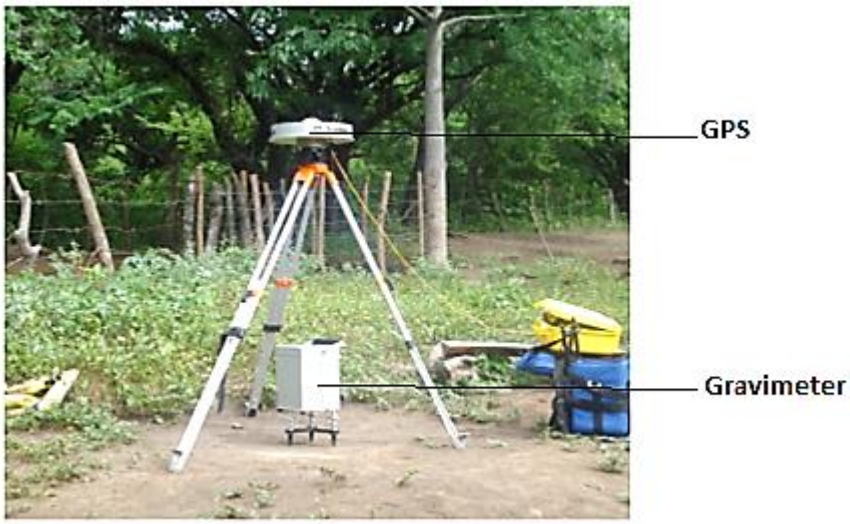

Figure 4.1 Opening of gravity base station

The total gravity data employed in this study are 1230 observations as shown in the Fig 4.2 by a doted point and the blue lines are the profile lines. Of these the 400 data are collected at a station interval of 2km along roads and tracks. The remaining data were obtained from Geological Survey of Ethiopia.

The routine gravity data collection is looping system. Reading started and ended at the base stations that were established at every 10km throughout the surveyed area. Reading

at base stations was repeated every two hours to determine drift. The secondary gravity base stations located at Abomsa and Gelemso were used to tie each gravity station reading with the gravity base net of the country. Every day gravity data reading started and ended at the base station. At each station the gravimeter reading, reading time, the coordinates and elevation were recorded.

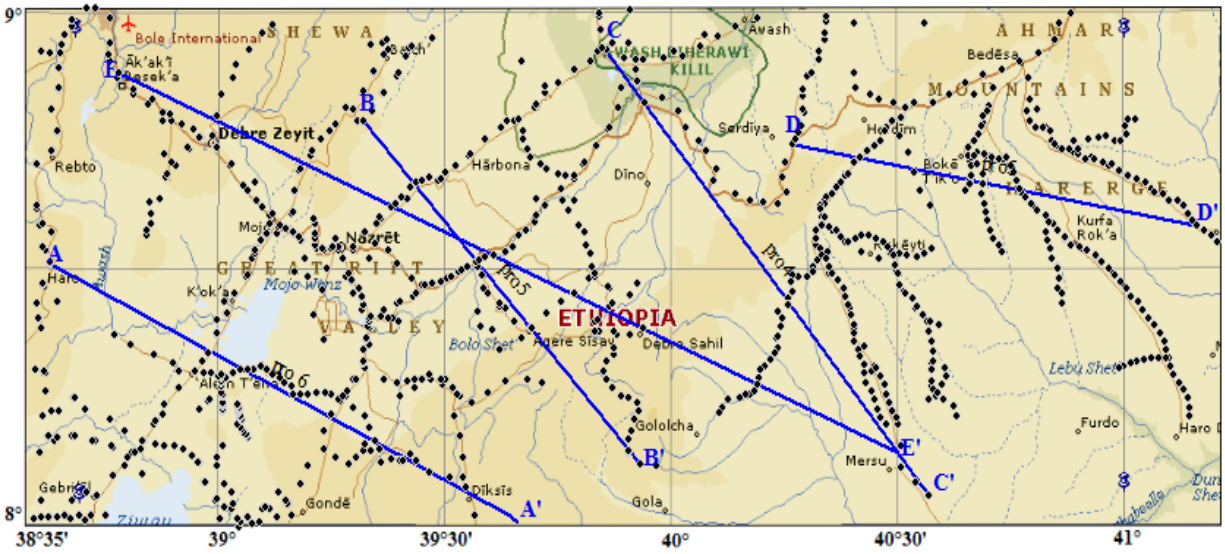

Figure 4.2 Distribution of gravity station under the study

The gravity data were adjusted to the International Gravity Standardization Network 1971 (IGSN71) and reduced using the Geodetic Reference System 1967 (GRS67).

4.2 Data reduction

The raw gravity data are affected by a wide variety of sources of varying amplitudes, periods, and wavelengths that generally mask gravity variations of geologic or geophysical interest. As a result, field observations are processed to minimize these extraneous effects. This conversion procedure is commonly referred to as correction or reduction of the gravity data. Correction does not imply that errors are present in the data, and reduction does not suggest that the data are reduced to a common vertical datum; but both terms refer to the conversion of raw gravity observations to anomaly form. A gravity anomaly is the difference between the observed gravity and the theoretical gravity value at the station. The observed value is a conversion of the raw gravimeter measurement to the absolute gravity at the station, corrected for temporal variations using ties to stations of known gravity; the theoretical value

of gravity at a station takes into account planetary and topographical gravitational effects. Free-air and Bouguer gravity corrections were made using sea level as a datum and 2.67 gm/cc as a reduction density. The merged gravity anomaly data were gridded at a spacing of 1.5 km using the minimum curvature technique and contoured at a ten mGal interval to produce a Bouguer gravity anomaly map (Fig 4.6).

4.2.1 Free Air Anomaly Map

The free air correction accounts for gravity variations resulted from elevation differences in the observation locations. Here the attraction of materials between the station and the reference ellipsoid will not be taken into consideration. Because of this, the variation is known as free air anomaly. Thus, this free air anomaly is given as

$$\Delta g_{FA} = g_{obs} - (g_N - 0.3086h)(\text{mgal}) \qquad (4.1)$$

where, g_{obs} - Drift corrected observed gravity

g_N - Normal gravity

h - Elevation (in meters)

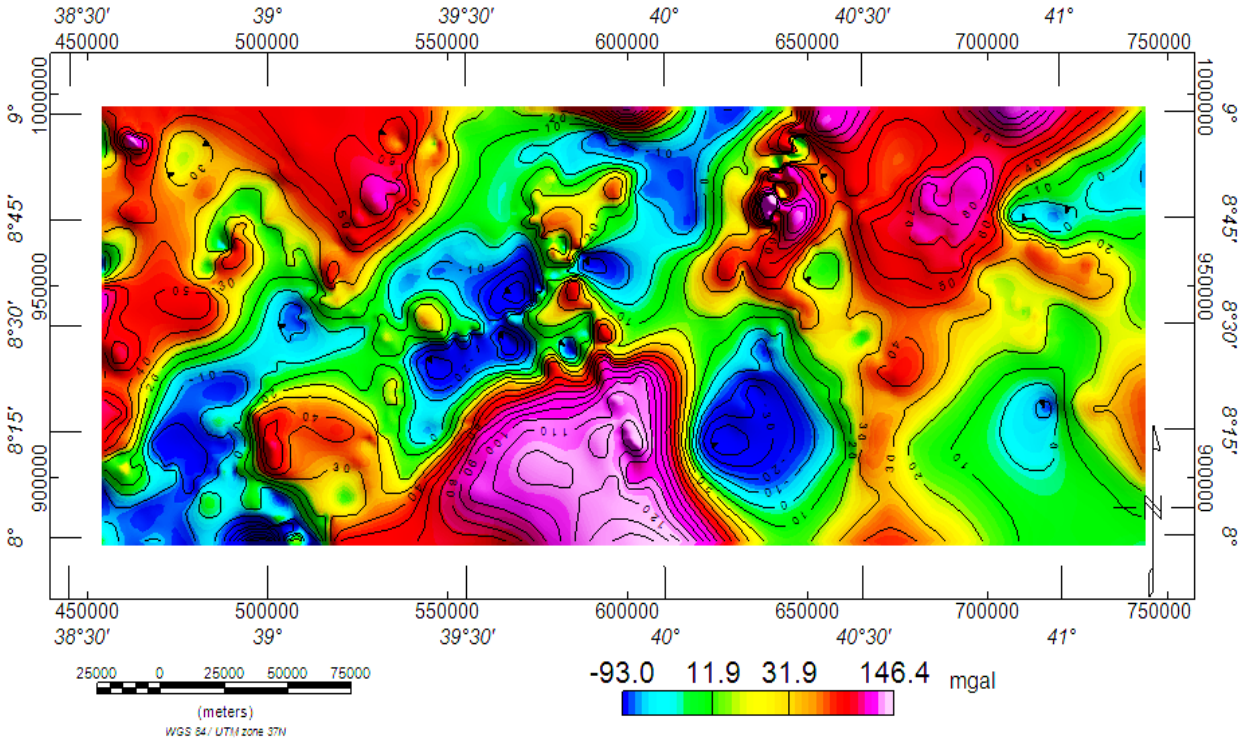

Figure 4.3 Free Air anomaly map of the study area

The contor interval for free air anomaly (Fig 4.3) and elevation maps (Fig 4.4) are 10 mgal and 100 meter respectively. These contour interval are arbitrary but should be chosen so that the contour map shows the geologic pattern clearly without being crowded with too many contour lines. In general contour interval chosen for a map depends on the topography in the mapped area.

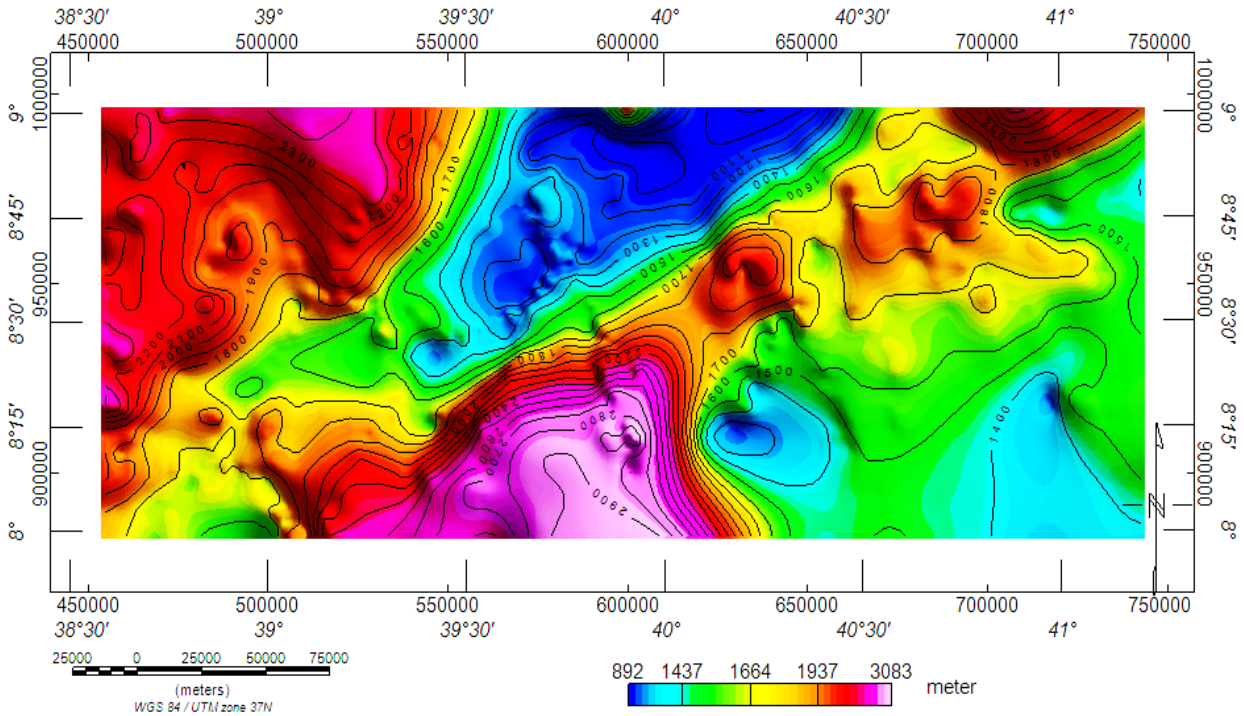

Figure 4.4 Elevation map of the study area

The free air anomaly map of the study area shows a strong positive correlation with the elevation map (Fig 4.3 and Fig 4.4). The maximum values of elevation and free air anomaly map are found at the rift margin with values 3083 m and 146.4 mGal respectively. The minimum value for the elevation map 892 m and -93 mGal for free air anomaly map are observed at the rift center and some parts of eastern plateau. The free air anomaly map is produced by Geosoft Oasis Montaj software and this anomaly in general shows the distribution and vertical gradient of the gravity field on the surface of the earth.

4.2.2 Complete Bouger Anomaly map

The Bouguer anomaly is the difference between the measured value at the point of observation and theoretical value calculated for that elevation or water depth by

considering a Bouguer slab of appropriate density for the effect of the earth's material between the geoid and the station. The Bouguer anomaly calculated by ignoring topographic effects is known as Simple Bouguer Anomaly (SBA)

$$\boldsymbol{SBA = g_{obs} + 0.3086h - 0.1119h - \gamma} \quad (4.2)$$

When all the corrections, the free air, Bouguer and terrain corrections are applied to the observed gravity, the resulting anomaly obtained by subtracting the standard theoretical gravity at the given latitude is known as the Complete Bouguer Anomaly (CBA).

$$\boldsymbol{CBA = g_{obs} + 0.3086h - 0.1119h + \delta g_t - \gamma} \quad (4.3)$$

Where, δg_t- Is the terrain correction factor.

The main outcome of gravity work is the Bouguer anomalies, which should correlate with lateral variations in the density of the upper crust. On the continental platform, the Bouguer anomaly is generally less than zero and is strongly negative on high mountains. This is due to the mass deficit that exists beneath the continents causing the negative Bouguer anomaly. The mass distribution underneath the observation point could be shallow or deep in origin. Shallow origin mass distributions are subsurface anomalous masses with lateral density variations. Subsurface anomalous masses gives rise to negative or positive Bouguer anomalies depending on their density contrast with respect to the mean crustal density ($2.67 g/cm^3$) used in the Bouguer reduction (Dobrin, 1988). The lateral extent of the Bouguer anomalies due to subsurface anomalous bodies is small compared with those of Bouguer anomalies of deep origins. In general the Bouguer anomalies on a local scale are caused by the lateral variation in density of the sub surface masses. On the other hand the non-homogeneous crust of variable density and thickness causes the anomaly on a regional scale.

The Bouguer anomaly values (Fig 4.6) range from a minimum of -259 mGal at the NW and southern end of the western half of the area to a maximum of about -32 mGal at the northern part. The Bouguer anomaly obtained is due to both shallow and deep origin mass distribution. Referring to the Bouguer anomaly map (Fig 4.6) the eastern part of the area generally shows a relatively higher Bouguer anomaly values than the western part. Along the NE-SW rift lineament there is a gradual increase in the gravity value towards the North East to the southern part of Afar region.

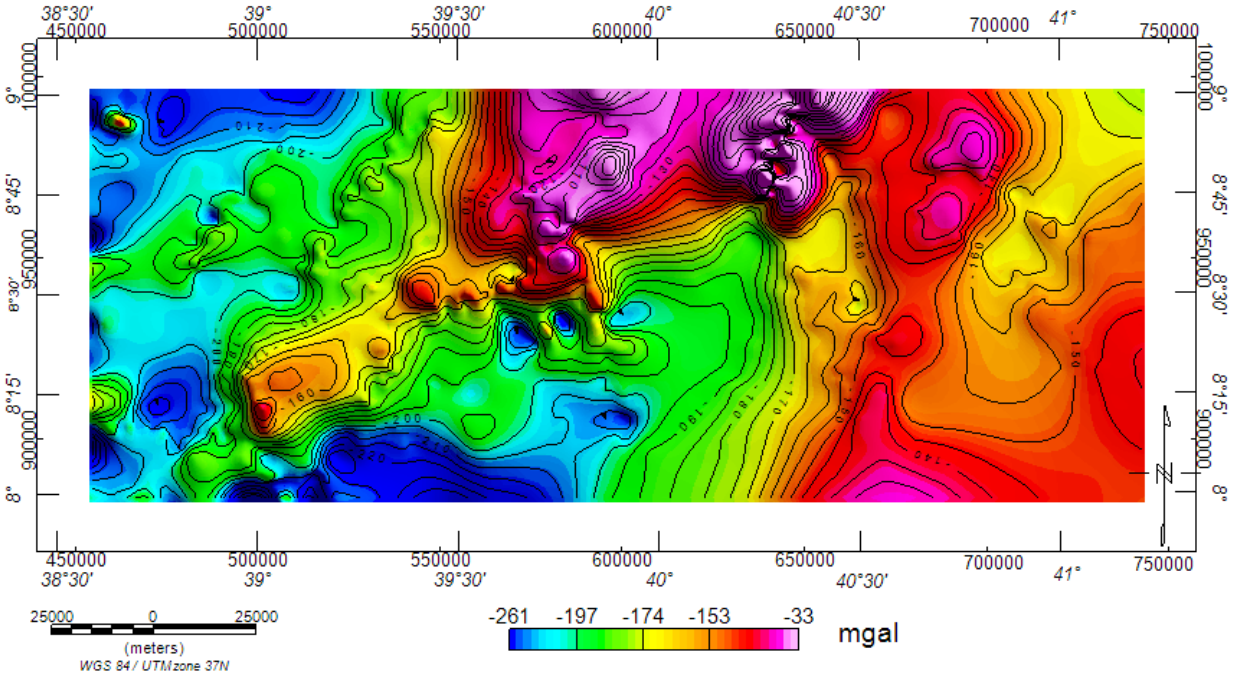

Figure 4.5 Simple Bouguer Anomaly map

.

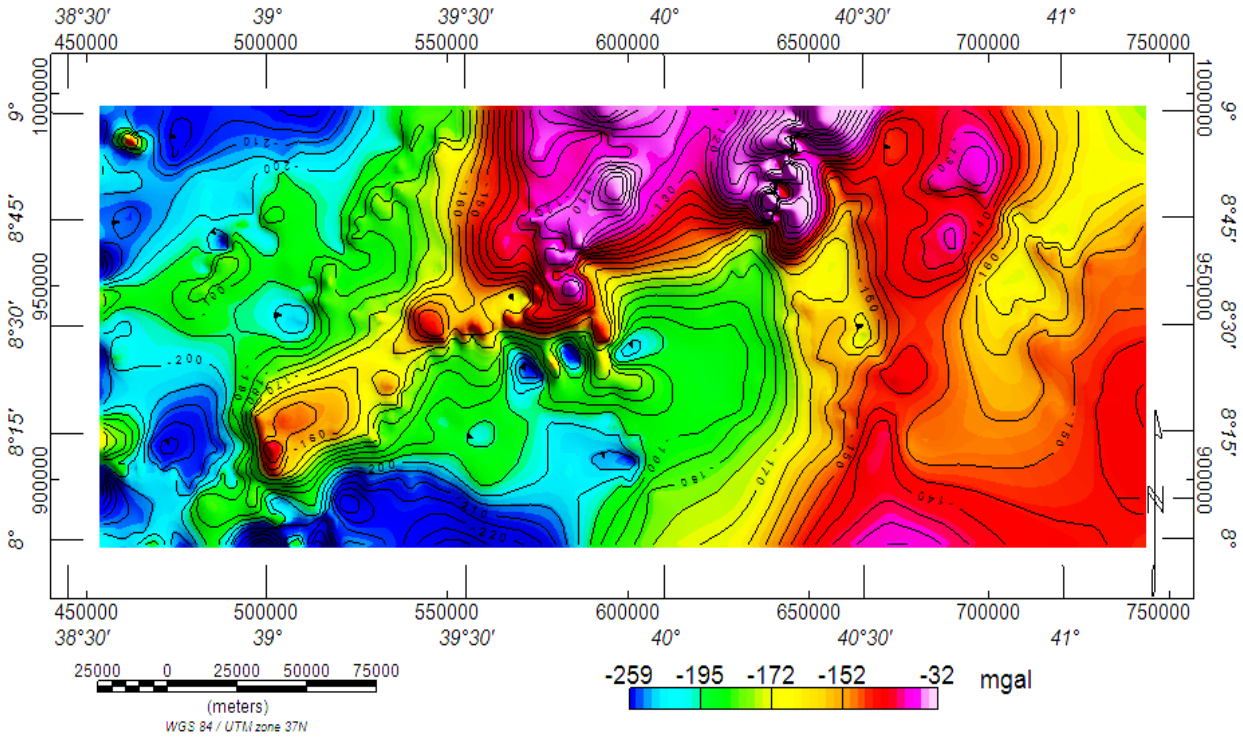

Figure 4.6 Complete Bouguer Anomaly map

Mickus et al. (2007) associated this gradual increase in gravity value to a thinned crust, igneous intrusion or a combination of both. This observation was also noted by Keller et al. (2004), who explained the crustal depth variation from 40 km in the central MER to 30 km in the southern Afar region.

4.3 Separation of Regional and Residual Anomalies

4.3.1 Residual anomaly map obtained from second order polynomial fitting.

In order to study the gravity anomaly in detail, residual gravity anomaly maps have been constructed. There are varieties of techniques that can be used to estimate the regional gravity anomaly including polynomial fitting, wavelength filtering, etc. In this study The second order polynomial fitting is used to obtain the residual anomaly field. Large-scale, deep-seated structures on gravity maps dominate to an extent that it may be very difficult to recognize smaller or shallower features. Therefore, separation of the regional effect to obtain local features is very important.

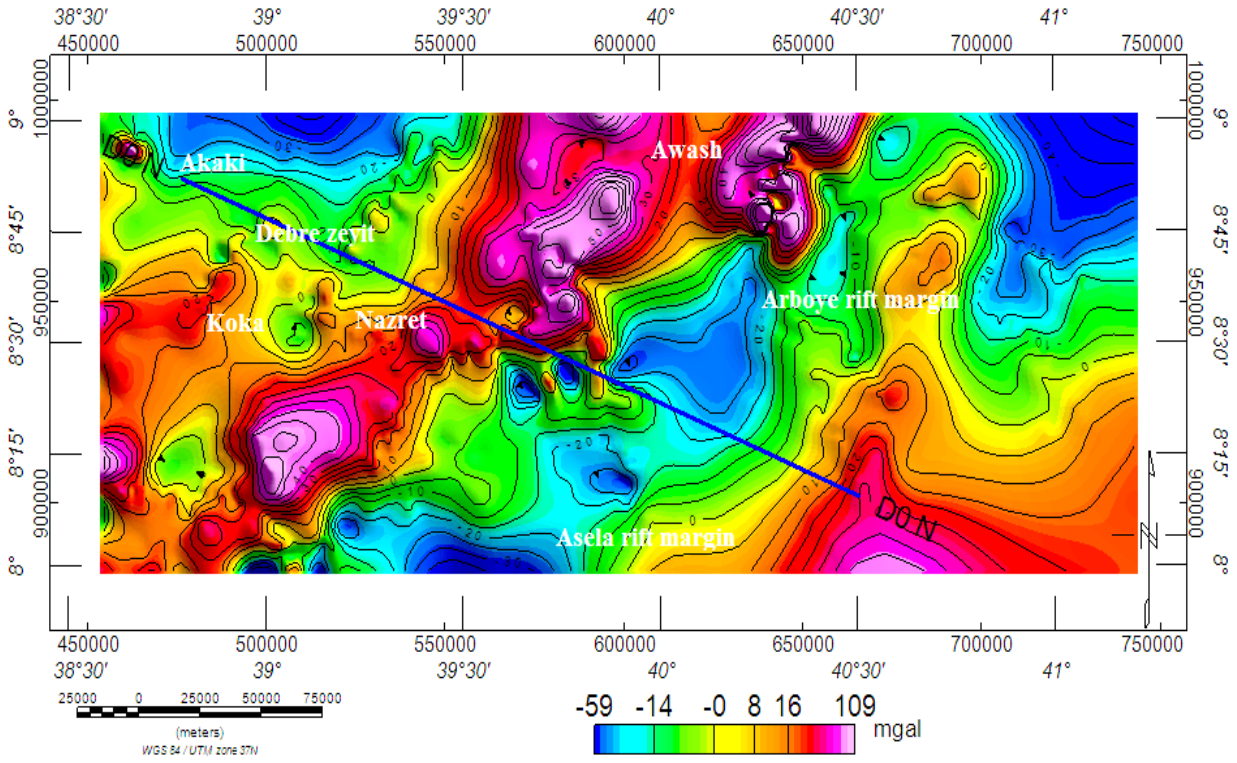

Figure 4.7 Second order residual gravity anomaly map constructed by removing the regional field

In the residual Bouguer anomaly map (Fig 4.7) the anomaly values range from a minimum of -59 mGal to a maximum of 109 mGal. The map reveals distinctive features that were

masked by the regional effect. The NE-SW rift lineament might be interpreted as the effect of high density material coming from the mantle intrude fault & fractures along the central rift and forming magmatic segments. This corresponds to the magmatic bodies modeled by Tiberi et al. (2005) that suggests the presence of a deeper dense features along the centeral rift. The SE part of the area also shows high gravity values that could be due to the presence of basaltic rocks. The remaining part of the area shows low gravity values possibly due to low density material and the high elevation of the rift margin.

4.3.2 Upward continued Complete Bouger Anomaly map

The principle of continuation is the mathematical projection of potential field data from one datum vertically upwards or downwards to another datum. Effectively, the continuation process simulates the anomaly at levels below or above sea level as if the data had been obtained at those levels. Upward continuation serves to filter out the shorter wavelength anomalies and reduce their amplitudes and decrease noise.

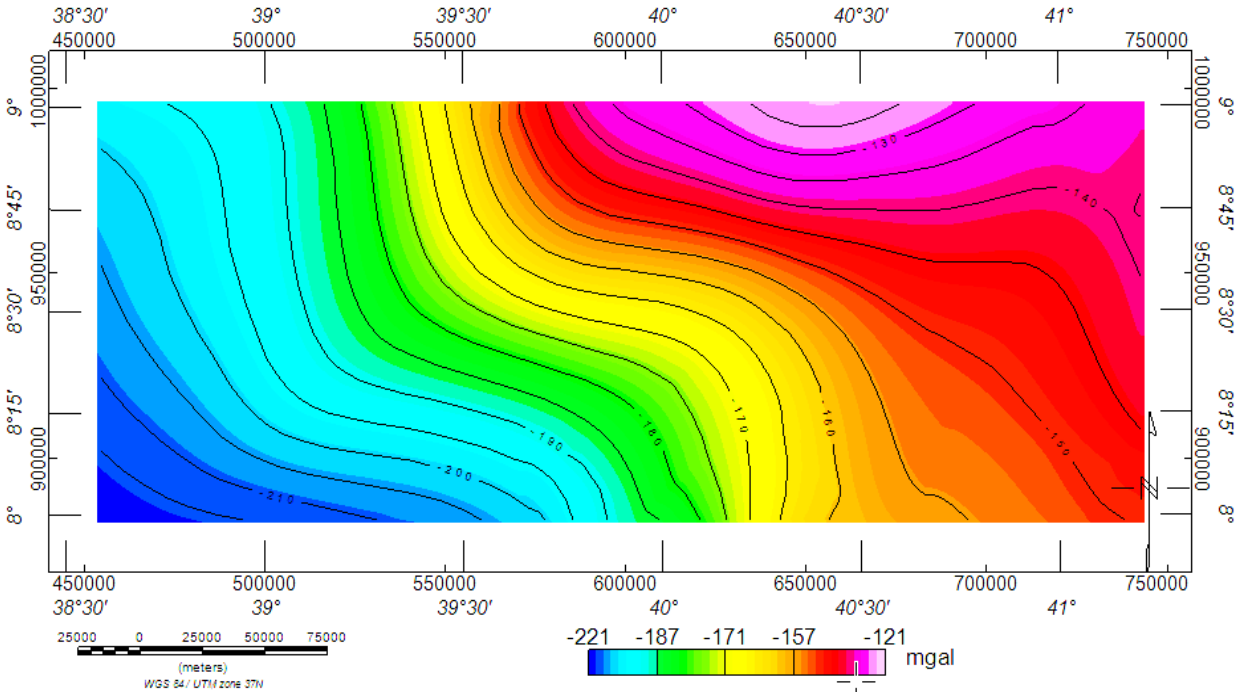

Figure 4.8 Upward continued Complete Bouger anomaly map to 30km

The upward continued map minimizes the effect of irregular shape anomalous features. A visual examination of Fig 4.8 indicate that the smooth trend of the anomaly that increase the value gradually form south western to the north eastern part of the study area. This

observation has been noted by Mahatsente et al. (1999) and Tiberi et al. (2005), who explain this increase as resulting from a decrease in the depth of the crust/mantle boundary and an increase in the crustal/upper mantle density to the north east along the rift (Keller et al., 2004).

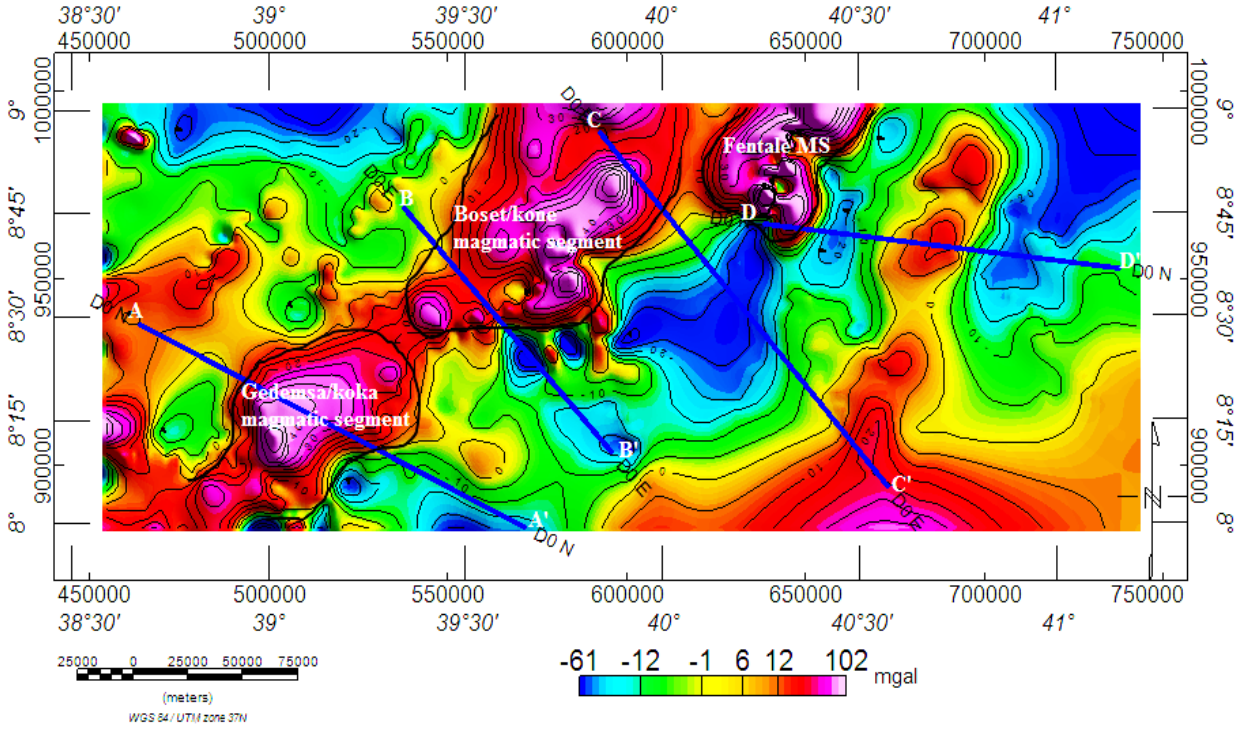

Figure 4.9 Residual gravity anomaly map obtained by subtracting upward continued map (up to 30km) from the complete Bouger anomaly map.

The residual anomaly map of Fig 4.9 was obtained by subtracting the 30km upward continued field from the complete Bouger anomaly map to get a residual gravity anomaly. The residual map thus obtained is generally similar to the residual map of Fig 4.7 obtained by removing second order regional field. The most obvious features of this map are the series of gravity maxima along the rift lineament. These gravity maxima may suggest the presence of dense intrusions beneath the volcanic centers. The blue lines on the map are the profile line.

CHAPTER FIVE

DATA ANALYSIS AND INTERPRETATION

5.1 Qualitative interpretations

5.1.1 Vertical derivative map (VD)

VD image maps help to resolve and emphasize the shallow source bodies. In VD anomaly maps the contour values close to zero may indicate the lateral edges of the source bodies (Xu *et al.*, 2011). The computation procedure is performed on a wave number domain using a Fast Fourier Transform. The definition of the VD operator is given by Blakely (1995) as follows:

$$F\left[\frac{\partial g}{\partial z}\right] = \lim_{\Delta Z \to 0} \frac{F(g) - F(g)e^{-|K|\Delta z}}{\Delta z} \tag{5.1}$$

$$= \lim_{\Delta z \to 0} \frac{1 - e^{-|K|\Delta z}}{\Delta z} F(g) \tag{5.2}$$

where g is the gravity field, e is the exponential function and $F(g)$ is the Fourier transformed grid data. Thus the first-order VD is equal to the Fourier transform of the potential times $|k|$, as given below Blakely (1995):

$$VD(x, y) = \frac{\partial g(x,y)}{\partial z} = F^{-1}\{|K|F(g)\} \tag{5.3}$$

where $F^{-1}$is the inverse Fourier transforms and $|k|$ is the radial wavenumberr at grid intersections throughout the K_x & K_y plane. $|k|$ is defined by the following equation Blakely (1995):

$$|K| = \sqrt{{K_x}^2 + {K_Y}^2} \tag{5.4}$$

The anomaly map produced by the VD filter (Fig 5.1) is somewhat similar to the residual gravity anomaly map of the area. As can be clearly seen, the dense intrusion zones which are interpreted in the residual anomaly maps were highlighted by positive anomaly values.

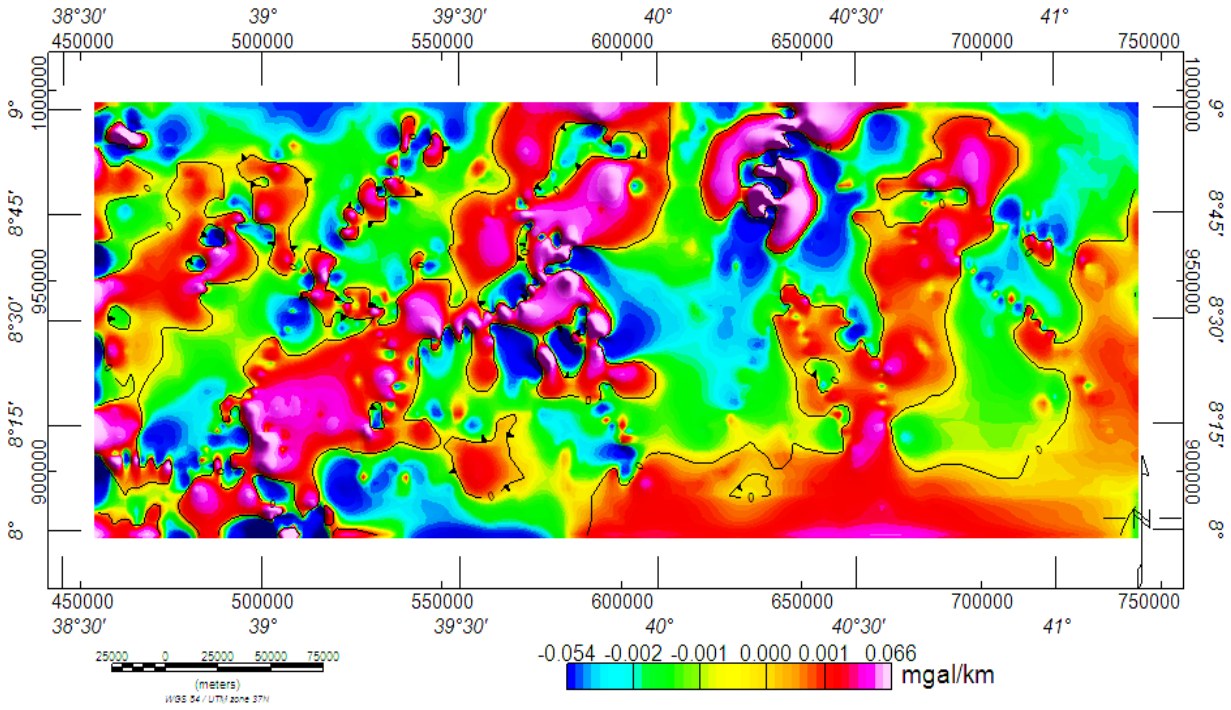

Figure 5.1 Vertical derivative map of complete Bouger anomaly map

The NE–SW direction along the rift and SE part of the study area produces positive anomaly values. In general the zero contour value which is consistent with high gravity value may indicate the edges or contact of the causative bodies.

5.1.2 Horizontal gradient map

The usual method for detecting edges in the potential field data is the horizontal gradient magnitude. The horizontal gradient map is simple and intuitive derivative product to reveal the anomaly structure of potential field maps and to highlight discontinuities in the anomaly pattern. The horizontal and vertical gradients are often used to highlight subtle features, as well as accentuate discontinuities and breaks in anomaly trends. In general, anomalies exhibited by horizontal-gradient map maxima occur over the steepest parts of potential field anomalies, and minima over the flattest parts (MA zong-Jin et al.,2006).

The high gradient zone along NE-SW of rift lineament as shown in the Fig 5.2 shows the main part of the central rift. The edge of this trend highlighted by the white line may possibly indicate the rift margin (border fault).

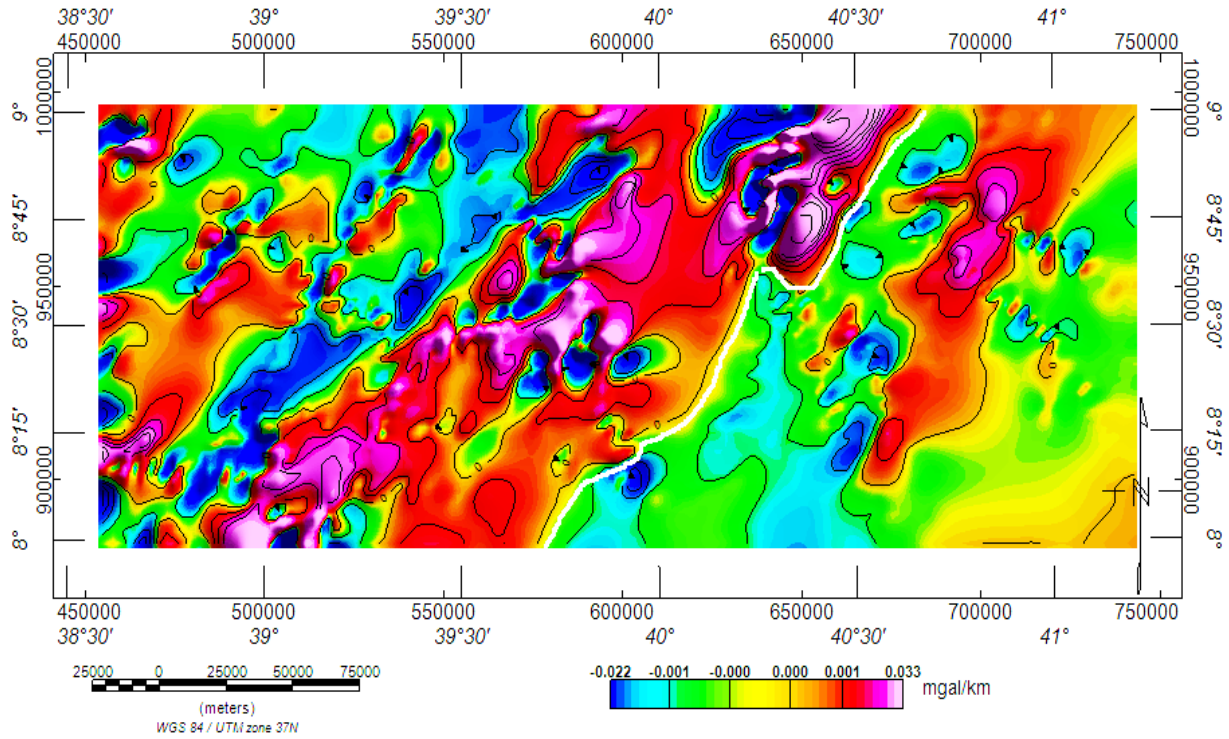

Figure 5.2 Horizontal gradient map counterclockwise at 135°

The E & SE part of the study area shows low gravity gradient which is consistent with the description by Lyatsky et al. (2005), who noted that the gradient values of the anomaly is low at flattest part and high in slope area.

5.1.3 Analytic signal (AS) map

The AS amplitude is a complex quantity formed through a combination of the horizontal and VDs (vertical derivatives) of the potential field data. The maxima locations in the AS anomaly map are used to locate the lateral edges of source bodies on the grid plane. The equation for the AS amplitude is given by Roest et al. (1992) as follows:

$$AS(x,y) = \sqrt{\left(\frac{\partial g}{\partial x}\right)^2 + \left(\frac{\partial g}{\partial y}\right)^2 + \left(\frac{\partial g}{\partial z}\right)^2} \qquad (5.5)$$

where, g is the gravity field.

The amplitude of a simple analytic signal peaks over the geologic contacts or features (Nabighian, 1972).

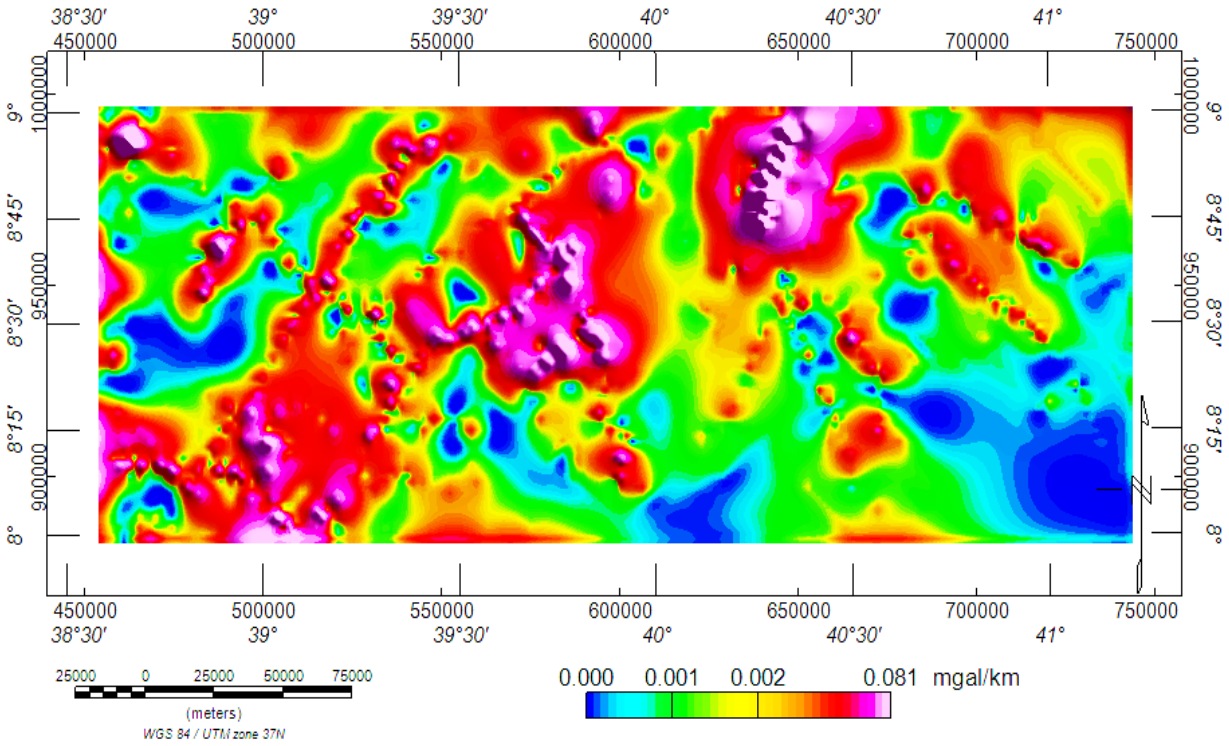

Figure 5.3 Analytic signal map

The analytic signal map of the study area is produced from trend two polynomial residual anomaly map. Close examination of the map contains the existence high amplitude responses (anomaly peaks) on the succession of NE – SW of the rift lineament. This result is clearly coincides with residual anomaly maps that shows the existence of an intrusion beneath the volcanic centers.

5.1.4 Tilt derivative

The tilt derivative operator can be briefly explained as amplitude normalized vertical derivative. Due to the nature of the arc tan trigonometric function, the output values of the procedure are limited to values between $-\pi/2$ and $\pi/2$. The tilt derivative operator uses the zero-point location to approximate the lateral edge location of causative geological bodies on the grid plane (Wanyin et al., 2009). Because the tilt derivative operator is based on the ratio of derivatives, it enhances both large and small amplitude anomalies well (Cooper and Cowan, 2008). The computation procedure of the tilt derivative operator can be expressed as the following equation (Miller and Singh, 1994), where g is the gravity field:

$$TA(x,y) = \tan^{-1}\frac{\frac{\partial g}{\partial Z}}{\left[\left(\frac{\partial g}{\partial x}\right)^2+\left(\frac{\partial g}{\partial y}\right)^2\right]^{\frac{1}{2}}} = \tan^{-1}\left[\frac{VDR}{THDR}\right] \quad (5.6)$$

where VDR is vertical derivative and THDR is total horizontal derivative.

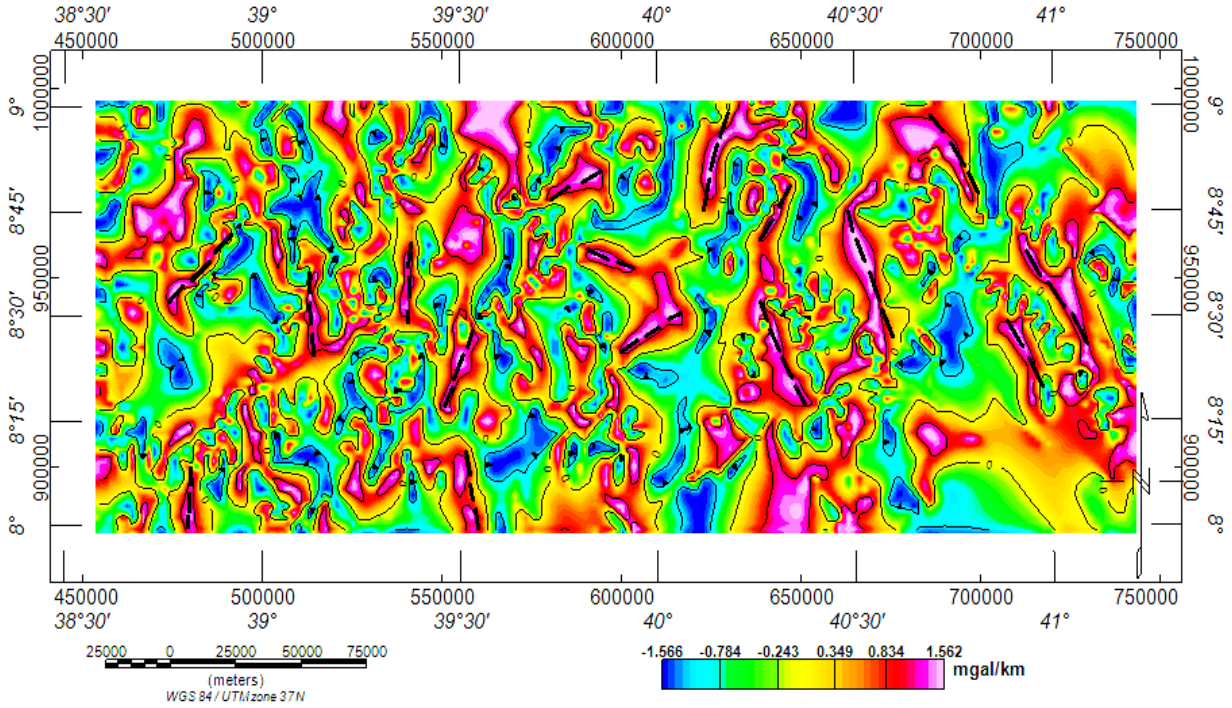

Figure 5.4 Tilt derivative map

Tilt derivative map showed considerably more detail than the residual gravity anomaly map. The zero contours of the tilt derivative map correspond to the boundaries of geologic discontinuities and are used to detect the linear features in the study area. The tilt angle produces a zero value over the source edges and, therefore, can be used to trace the outline of the edges (MILLER and SINGH, 1994). The black line on the map indicates geologic contacts/discontinuity of the study area.

5.1.5 3D Euler deconvolution

The objective of the 3D Euler deconvolution process is to produce a map showing the locations and the corresponding depth estimations of geologic sources of magnetic or gravimetric anomalies in a two-dimensional grid (Reid, 1990). The Standard 3D Euler method is based on Euler's homogeneity equation, which relates the potential field

(magnetic or gravity) and its gradient components to the location of the sources, by the degree of homogeneity N, which can be interpreted as a structural index (Thompson, 1982).

The method makes use of a structural index in addition to producing depth estimates. In combination, the structural index and the depth estimates have the potential to identify and calculate depth estimates for a variety of geologic structures such as faults, contacts, dykes, sills, etc.

The 3D equation for Euler deconvolution given by Thompson (1982) is

$$(x - x_0)\frac{\partial T}{\partial x} + (y - y_0)\frac{\partial T}{\partial y} + (z - z_0)\frac{\partial T}{\partial z} = N(B - T) \quad (5.7)$$

where (x_0, y_0, z_0) is the position of a source whose total field T is detected at $(x; y; z)$, and B and N are the regional value of the field and the structural index, respectively. Since our field is gravity the equation is given by:

$$(x - x_0)\frac{\partial g}{\partial x} + (y - y_0)\frac{\partial g}{\partial y} + (z - z_0)\frac{\partial g}{\partial z} = Ng \quad (5.8)$$

N is structural index and g is the first vertical derivative of gravity anomalies. The structural index defines the type of searched anomalous structure.

Table 5.1 Structural index of different geologic units at different potential fields

SI	Magnetic field	Gravity field
0.0	contact	sill/dyke/step
0.5	thick step	ribbon
1.0	sill/dyke	pipe
2.0	pipe	sphere
3.0	sphere	

The significance of the location and depth estimates obtained by 3D Euler Deconvolution is given by the specificity of the chosen parameters like the grid cell size, window size, structural index, chosen depth uncertainty tolerance, etc. The selection of the grid cell size

should be based on the grid spacing and the wavelength of the anomalies to be analyzed, as the software Geosoft Oasis Montaj allows a square window size of up to 20 grid cell units.

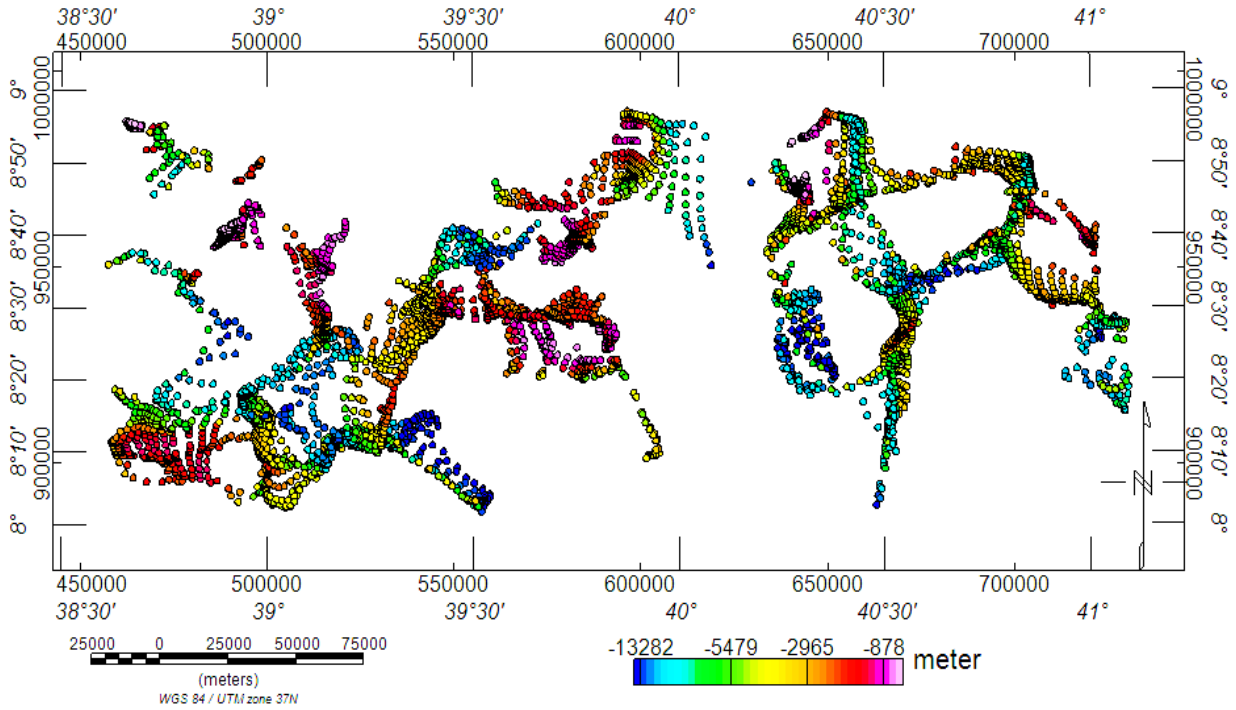

Figure 5.5 Standard Euler solution at SI-1.5

Euler deconvolution is a powerful method to gain preliminary information on position, shape and depth of causative bodies from gravity and magnetic fields. The Euler solutions outline different geologic structures. At higher values of SI (SI = 1 – 2), the solutions exhibited a clear focus in the location and depth of the anomalies, and results for these indices were shown in the Fig 5.5 and Fig 5.6. Generally, the solution of Euler deconvolution show that the depth range between 878 to 13282 meters for SI = 1.5 and 450 to 16329 meters for SI = 2. The Euler solution maps presented on Fig 5.5 and Fig 5.6 indicate several structures, with a direct correlation with features interpretd in residual anomaly map as intrusions, which is seen in the Fig 5.7. The north east – south west feature in the Fig 5.5 & Fig 5.6 with solutions extending to more than 450 m in depth suggesting that many of the sources are located close to or at the surface and some are deeper. The deeper one might be the magmatic intrusion along the rift lineament.

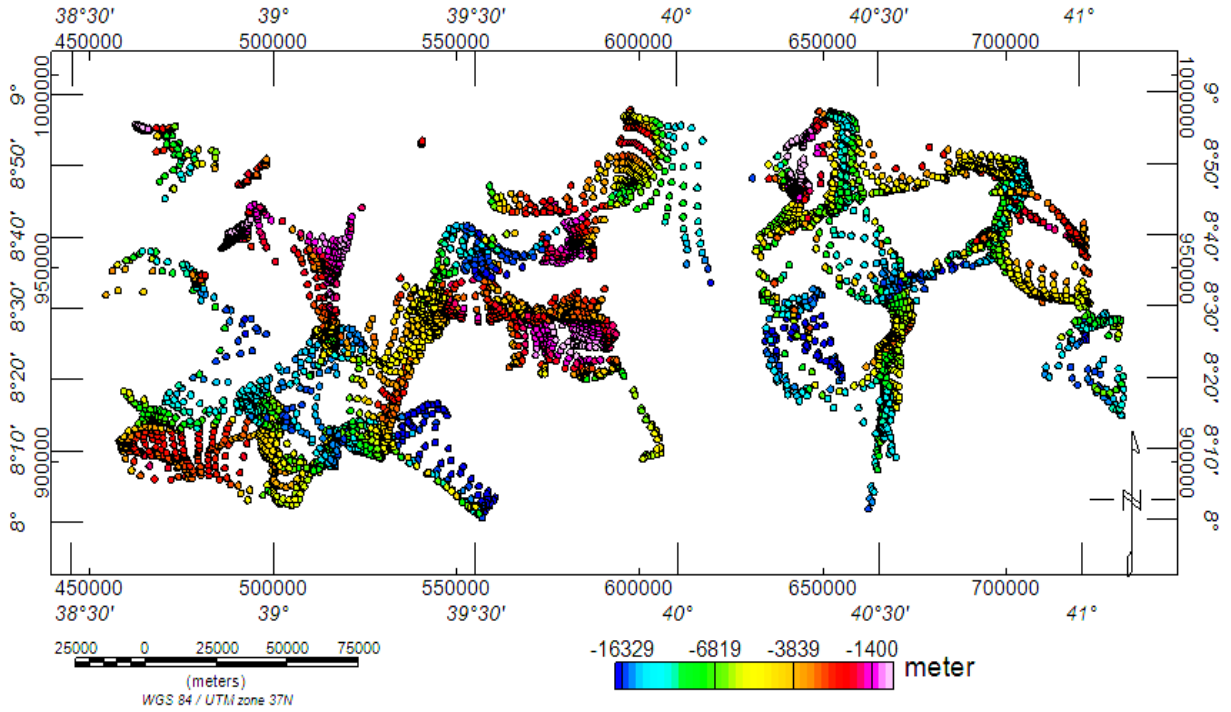

Figure 5.6 Standard Euler solution at SI-2

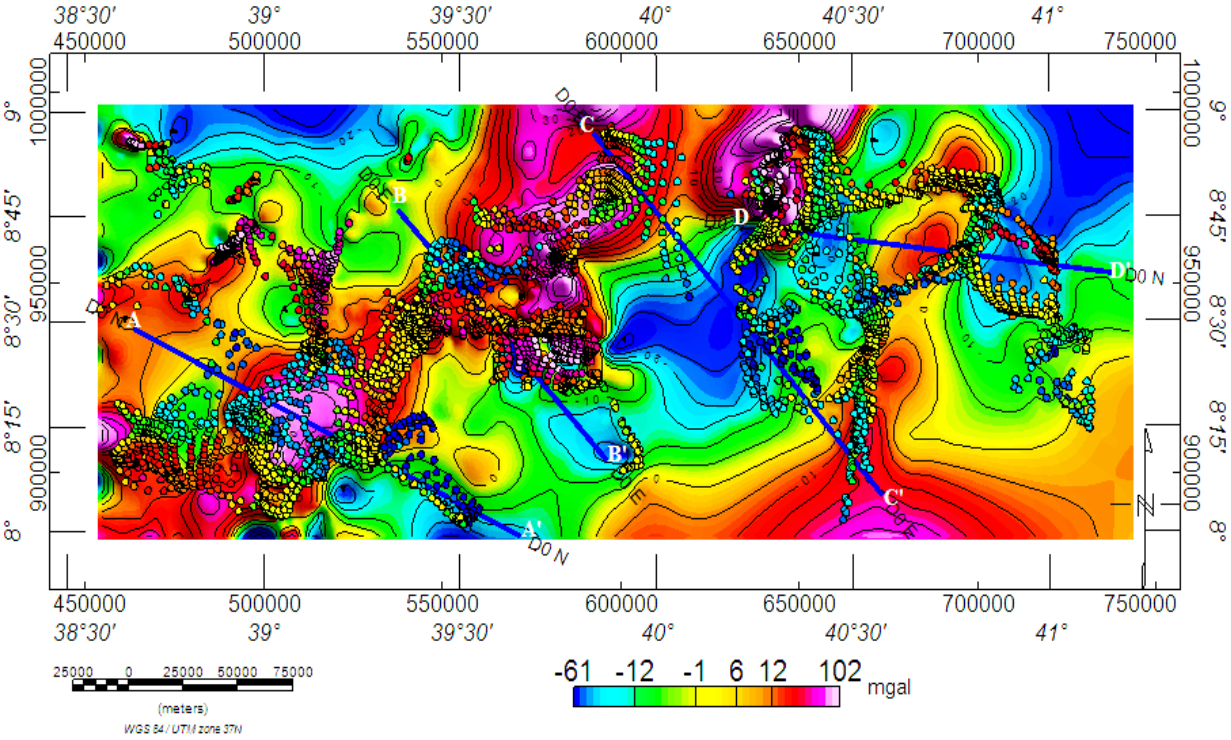

Figure 5.7 Standard Euler solution overlay on residual CBA

CHAPTER SIX

QUANTITATIVE INTERPRETATION AND DISCUSSION

6.1 Quantitative interpretation

6.1.1 Gravity forward modeling

The forward modeling of the gravity field has been done with GM-SYS 5.01.10 software which is an extension of GEOSOFT Oasis Montaj. GM-SYS is a modeling program that allows intuitive, interactive manipulation of geologic model and real-time calculation of gravity and magnetic responses. Forward modeling involves creating a hypothetical geologic model and calculating the geophysical response to the earth model. For this study five profile lines were prepared for modeling subsurface crustal structures. From these profiles one profile has been selected to model the earth's layer up to upper mantle and the other profiles are used to model the earth's upper crustal structures up to 20 Km.

The modeling software calculates and displays the potential field responses from a user-defined geologic class selection and based on the least-squares best fit. The best fit of the calculated potential field (gravity and magnetic) values were generated from the proposed model section with the respective observed values while adjusting systematically varying the size, shape and density of the sections.

6.1.2 Initial model

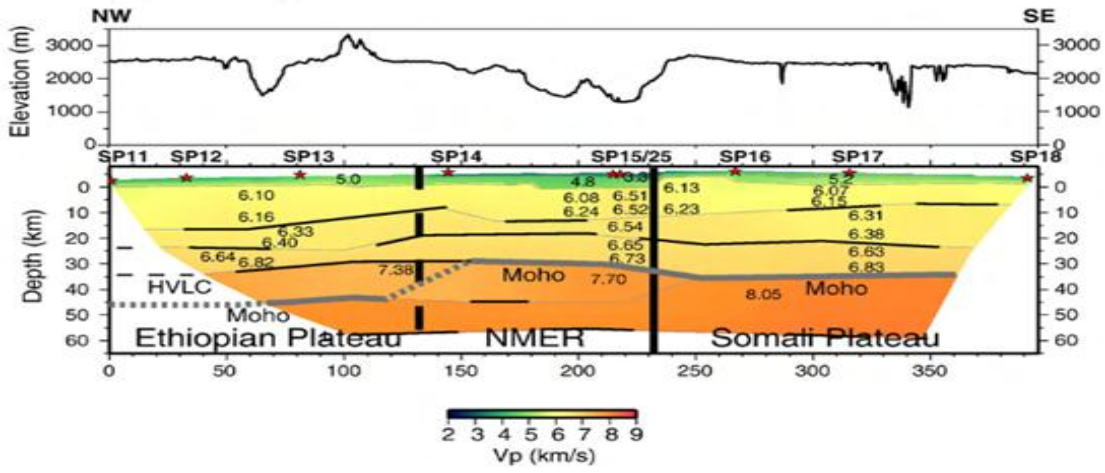

Figure 6.1 Cross-sections across the rift axis from the EAGLE controlled-source experiment, modified from (Maguire et al., 2006).

To constrain crustal thickness and density of subsurface structures EAGLE (Ethiopia Afar Geoscientific Lithospheric Experiment) controlled-source seismic refraction experiment were used for Profile EE'.

Correlations between compressional wave velocity (P – Wave) and density are important because they allow estimates of crustal density to be made for gravity modeling from seismic refraction velocities.

The initial density model was constructed by converting the highest and lowest velocity values in each seismic layer to a constant density polygon using a polynomial approximation of the best fit Nafe-Drake velocity-density relationship (Nafe & Drake, 1957)

$$\rho = -168.03 + 1765V_P - 481.72{V_P}^2 + 60.973{V_P}^3 - 2.6861{V_P}^4 \qquad (6.1)$$

where $\rho = density\ in\ Kg/m^3\ and\ V_P = P - wave\ velocity\ in\ Km/sec.$

Depends on equation (6.1) we can constrain the model density values from different P – wave velocities of Fig 6.1.

Table 6.1 Initial model from seismic refraction experiment

Layer	V_P (km/s)	$V_P - \rho$ relation (gm/cm^3)	model density (gm/cm^3)	thickness (km)
Volcanics and Sediments	3.3 – 5.2	2.28 – 2.59	2.57	0 – 6
Upper Crust	6.07 – 6.52	2.78 – 2.90	2.79	6 – 22
Lower Crust	6.54 – 6.83	2.91 – 2.99	2.94	22 – 39
Mantle	7.38 – 8.05	3.16 – 3.35	3.3	> 39

The initial densities and geometries were varied by up to 15% in order to obtain a final gravity model. The modeled sections for the other profiles were prepared based on prior information on the general stratigraphy of the study area shown in the Fig 6.2.

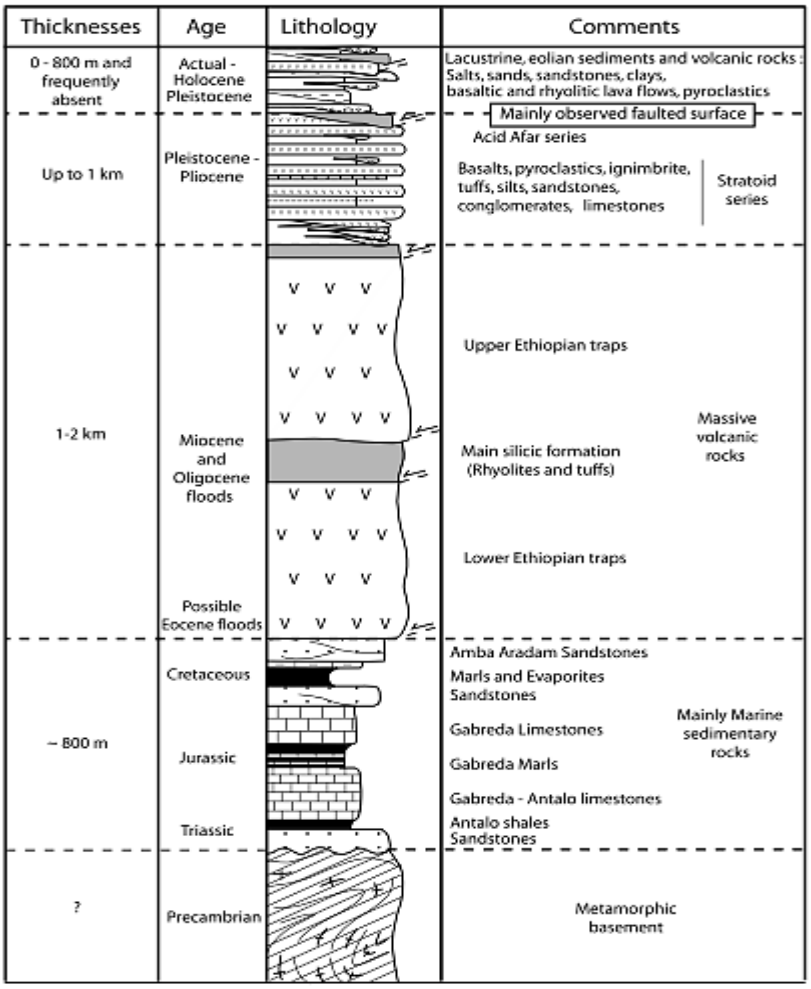

Figure 6.2 Synthesis of the stratigraphy in the MER-Afar transition area (Soliva and Schultz, 2008)

Table 6.2 Density values of different rock types

Rock types	*Density range* (gm/cm^3)
Sandstone	1.61 – 2.76
Shale	1.77 – 3.2
Limestone	1.93 – 2.90
Basalt	2.70 – 3.3
Acidic igneous	2.30 – 3.11
Metamorphic	2.40 – 3.10
Basic igneous	2.09 – 3.17
Intrusion strong (cooled)	2.80 – 3.00

6.2 Interpretation of the models

The Bouger residual anomalies are used in the modeling sections to assist in the interpretation of subsurface geologic structures. However, the modeling of the potential

field data can be complex due to the non-uniqueness (Blakely, 1995). This can be minimized by constraining the models with other geological and geophysical works.

The final subsurface models produce good fits between the observed and calculated anomalies. The fits were quantified by a Root Mean Square (RMS) error, which is computed by the software.

6.2.1 Model along profile AA'

The profile lies along NWW – SEE orientation that extends through Asela sire border fault. The model produce a suitable fit with the observed gravity data with root mean square error (RMS) of 1.162 mGal.

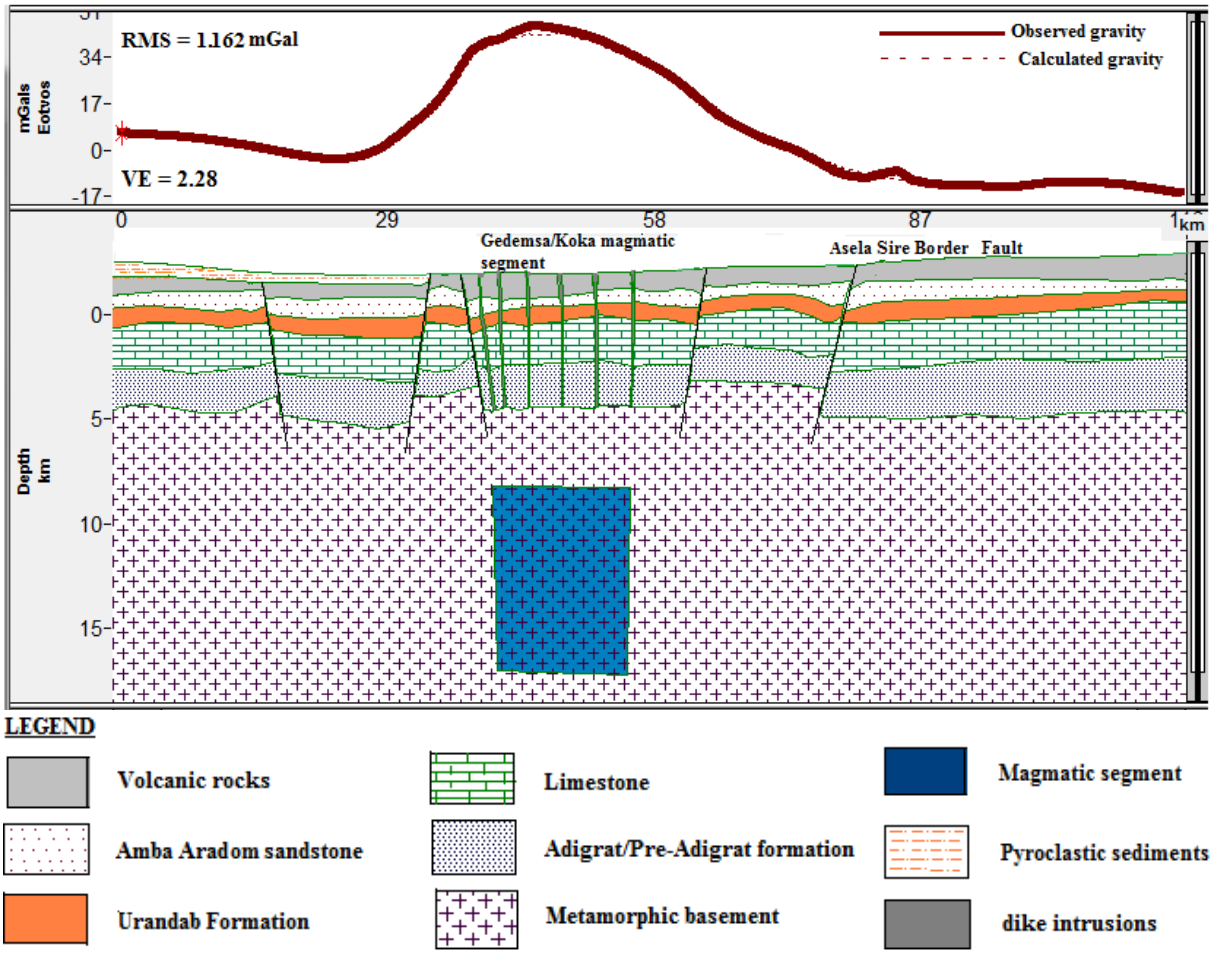

Figure 6.3 Model along profile AA'

Figure (6.3) shows different lithology along the profile with different density values and geologic structures. The NWW end of the profile contains pyroclastic sediments which overlying the volcanic rocks. The sediments have density of 2.5 gm/cm^3 and thickness of 100 – 150 m. Volcanic rocks outcrop along the profile at about 35 km from A. They are 1.5 – 2 km thick and have density value of 2.57 gm/cm^3. The Amba Aradom sandstone underlie the volcanics and has a density value of 2.4 gm/cm^3 and thickness ranging from 0.4 – 0.6 km. The underlying Urandab Formation has density value 2.45 gm/cm^3 and interpreted thickness of 0.6 – 0.8 km. The limestone beneath the Urandab Formation has thickness of 2 – 3 km and density of 2.52 gm/cm^3. The pre Adigrat/Adigrat Formation has thickness of 1.5 – 2 km and density value of 2.57 gm/cm^3. The Precambrian basement has an average depth of 5 km and a density value of 2.57 gm/cm^3. The Gedemsa magmatic segment is modeled at depths 8 – 16 km.It has an approximate width of 18 km which is close to the 20 km width estimated by Casey et al. (2006). The dike intrusions modeled beneath Gedemsa magmatic segment are an indicator for the presence of crustal extension in the NMER and has a density value of 2.8 gm/cm^3.

6.2.2 Model along profile BB'

The profile is oriented NW – SE and extends through the Asela sire border fault. The model produces a suitable fit with the observed gravity data with root mean square error (RMS) of 1.901 mGal.

Figure (6.4) shows more or less the same lithology as that of the model along profile AA'. The upper layer consists of volcanic rocks with thickness of 1.5 – 2.8 km & density value of 2.57 gm/cm^3. About 2.4 – 3 km thick sedimentary underlay volcanic rocks. The high amplitude long wave length gravity field indicate the Boset magmatic segment. The segment is 65 km long, steps 15 km to the east, and lies $\sim 500\, m$ lower than, Gedemsa magmatic segment (Casey et al., 2006).

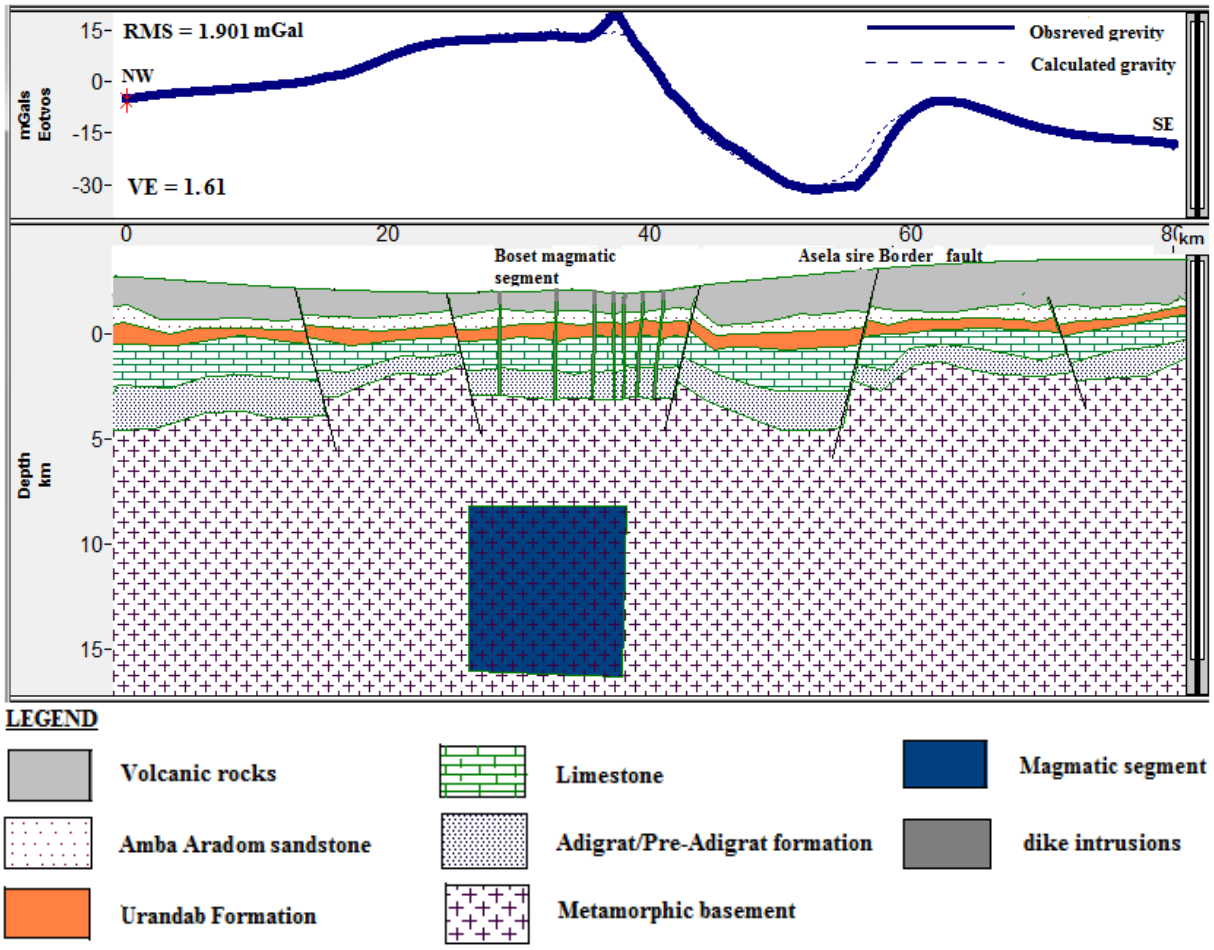

Figure 6.4 Model along profile BB'

6.2.3 Model along profile CC'

This profile lies along NW – SE orientation that extends through the eastern plateau. The modeling produces a suitable fit with the observed gravity data and the root mean square error (RMS) is 1.571 mGal.

Figure (6.5) shows that the top layer from Boset magmatic segment to Western part of the Arboye border fault is characterized by volcanic rocks that have a thicknesses of 0.8 – 1.2 km and density value 2.57 gm/cm^3. After Arboye border faults the Amba Aradom sandstone outcrops. It has variable thickness ranging from 0.4 to 1.5 km with density value of 2.4 gm/cm^3. Urandab Formation outcrops in the eastern plateau. The modeled thickness and density of Urandab Formation are 0.5 – 1.2 km and 2.45 gm/cm^3 respectively.

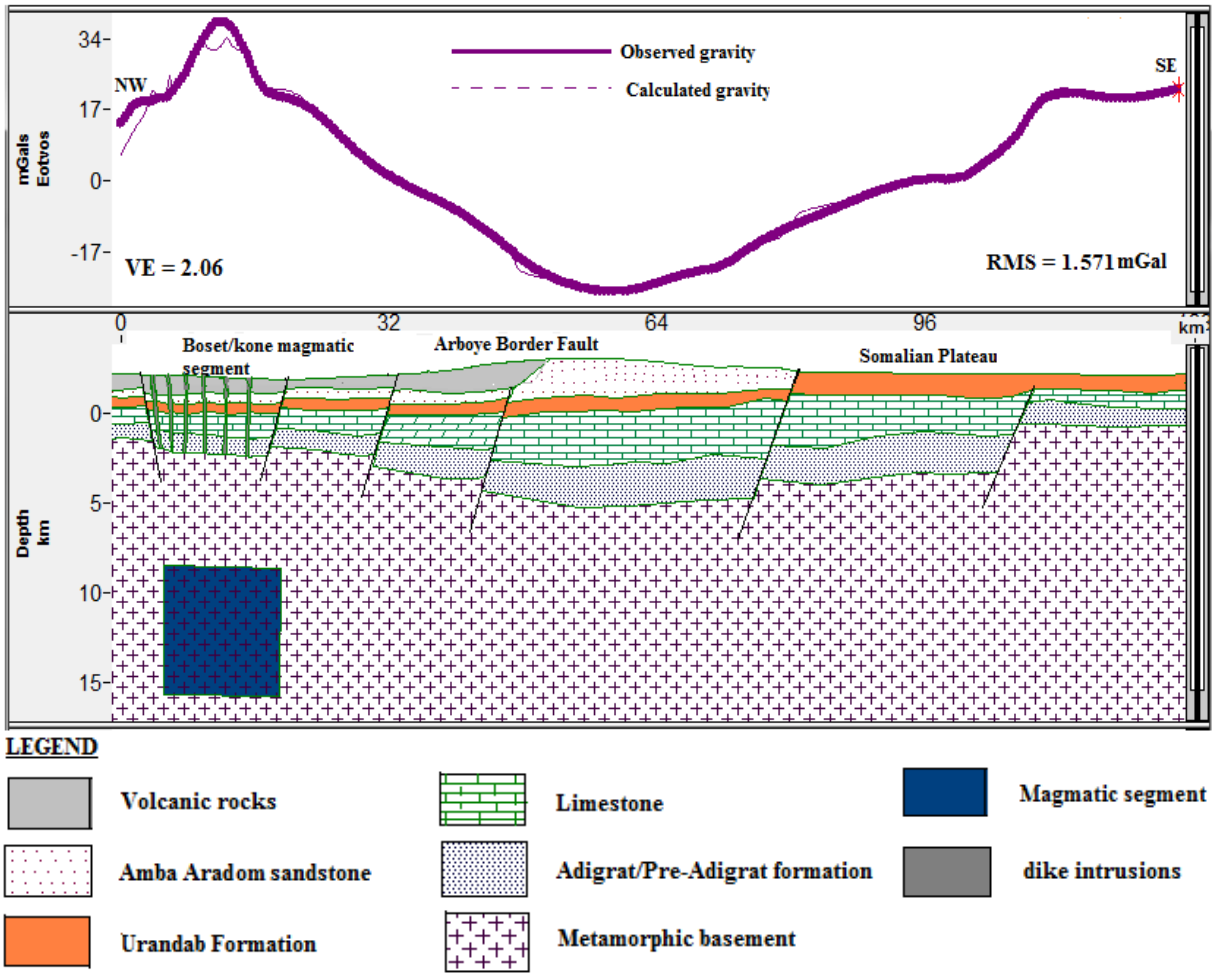

Figure 6.5 Model along profile CC'

The underlying limestone has thickness of 1 – 3.5 km and density of 2.52 gm/cm^3. The pre Adigrat/Adigrat sandstone is about 0.8 – 2.6 km thick and has density value of 2.57 gm/cm^3. An intrusive body (the Boset magmatic segment) is modeled at depths of 8 – 16 km with density 3.0 gm/cc.

6.2.4 Model along profile DD'

This is an E – W profile that extends through eastern plateau. The model produces a suitable fit with the observed gravity data with root mean square error (RMS) of 5.219 mGal.

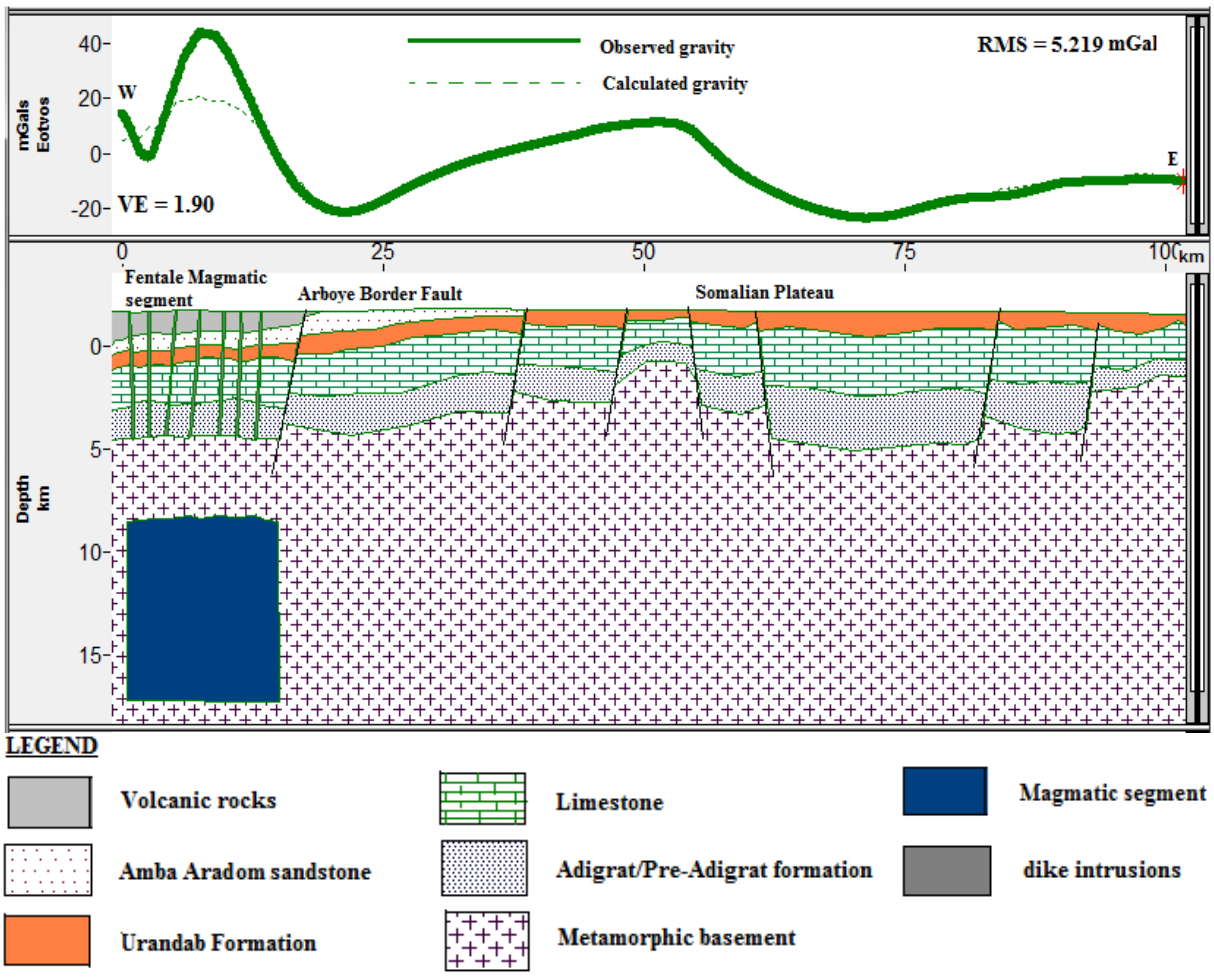

Figure 6.6 Model along profile DD'

Figure (6.6) shows that the top layeris similar to the model of profile CC'. The volcanic rock that extends from Fentale magmatic segment to the western part of Arboye border fault has interpreted thicknesses of 0.5 – 1.1 km and density value of 2.57 gm/cm^3. Unlike the Aluto – Gedemsa and Boset – Kone magmatic segment to the south, the Fentale – Dofen magmatic segment lies within a half – graben bounded along its Eastern side by a series of 60 – 80 m high scarps. This magmatic segment is marked by felsic shield volcanoes with elongate calderas at both its southern (Fentale) and northern (Dofen) ends (Casey et al., 2006). The Amba Aradom sandstone outcrops at the Eastern part of Arboye border fault. The interpreted thickness of the Amba Aradom sandstone is 0.7 km at the Fentale magmatic segment to 0.9 km at the eastern part of Arboye border fault and has density value of 2.4 gm/cm^3. The underlying Urandab Formation outcrops at the eastern

plateau. The interpretd thickness of this layer is 0.8 – 1.3 km with a density of 2.45 gm/cm^3. The limestone which is beneath Urandab Formation has thickness of 1.7 – 2.77 km and density value of 2.52 gm/cm^3. The Adigrat / pre Adigrat Formations have a thickness of 1.5 – 2.2 km and density value of 2.57 gm/cm^3. The short wave length and high amplitude gravity at the western part was interpreted as an indicator of the presence of magmatic segment. The short wave length and low amplitude gravity field might shows the presence of geologic contact as previously described.

6.2.5 Model along profile EE'

This profile has NW – SE begins from western plateau and extends through eastern plateau. The model produces a suitable fit with the observed gravity data with root mean square error (RMS) of 2.912 mGal.

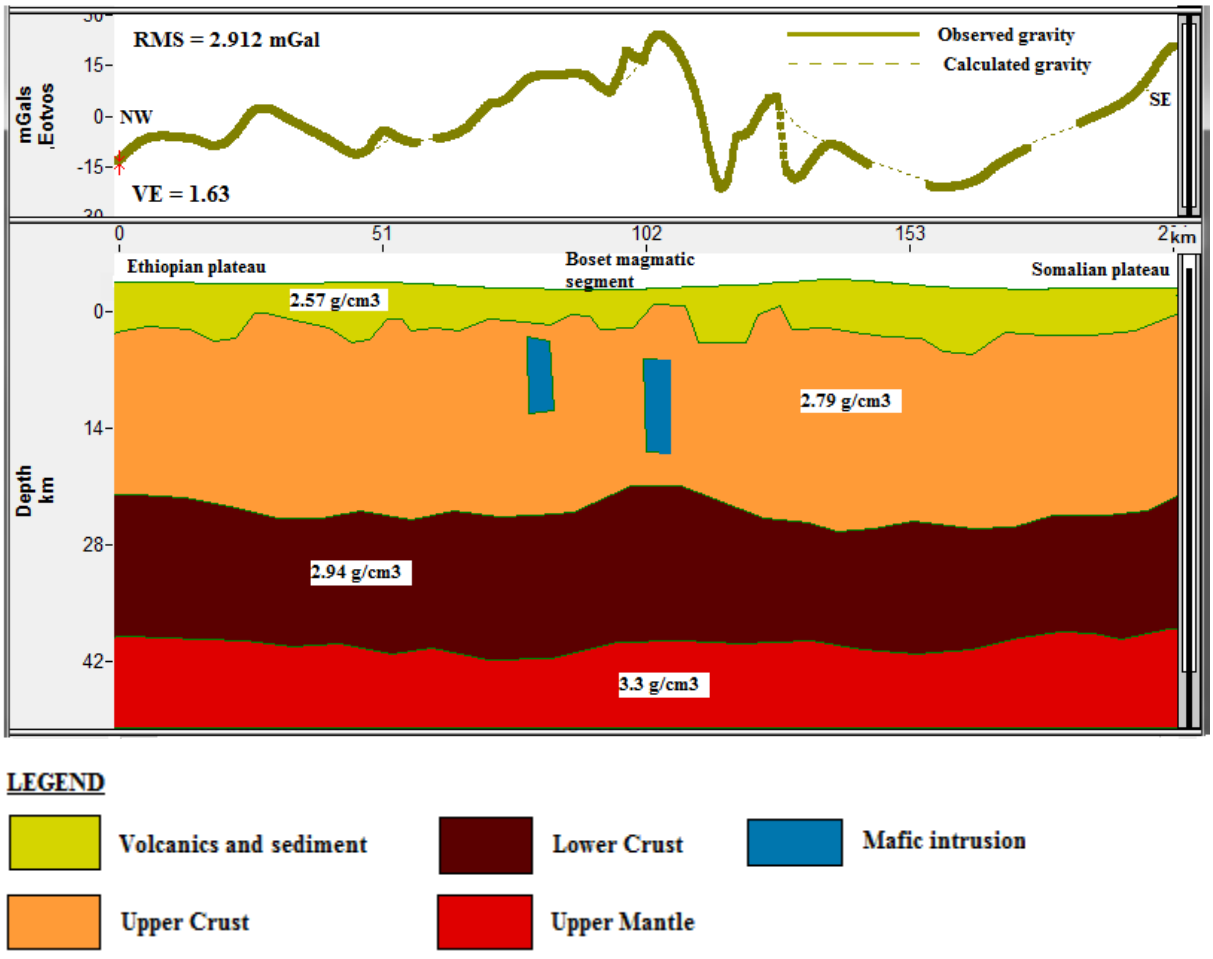

Figure 6.7 Model along profile EE'

Figure (6.7) shows four layers with intrusion in the upper crust and sediment in the top layer. The upper layer has thickness of 5 km and interpreted to represent interspersed quaternary lacustrine sediments, late Pliocene to early Pleistocene age pyroclastic deposits and late Miocene to Pliocene age pyroclastic rocks & Oligocene flood basalts (Wolfenden et al., 2004; Abebe et al., 2005) as well as Mesozoic sediments and has an average density value of 2.57 gm/cm^3. Beneath the volcanic rocks and sediments there is an upper crustal layer which extends down to depth 22 km. This layer is characterized by density value of 2.79 gm/cm^3. The lower crust has thickness of 22 – 39 km and density value of 2.94 gm/cm^3. The observed gravity anomaly exhibit a gradual increase in values from NW to SE consistent with a thick crust including a dense lower crustal layer beneath the western plateau and a thinner crust beneath the eastern plateau and central rift(Tiberi et al., 2005 ; Cornwell et al., 2006). The short wavelength gravity maximum on the observed gravity field may in general correspond to the magmatic segment and large volcanic centers. To model these small wavelength anomalies small blocks of intrusions were used under Boset magmatic segment. The density value for the intrusions is 3.0 gm/cm^3.

6.3 Discussion

The main objective of this study was gravity studies of the crustal structures beneath the Northern Main Ethiopian Rift and the adjoining eastern plateau. Previous geological and geophysical studies suggest the existence of magmatic segments (Maguire et al., 2006; Mickus et al., 2007; Wolfenden et al., 2004) beneath the MER. The research conducted in this study confirms the existence of the magmatic segments and revealed the general subsurface structure of the Main Ethiopian Rift. This study is an additional work to map the magmatic segments and the subsurface structures beneath both the magmatic segments between $8° - 9°$ latitude and the eastern border faults.

1. Border faults and magmatic segments

According to Corti (2009) strong uplift, resulting in the development of the Ethiopian and Somalian plateaus now surrounding the rift valley, has been suggested to have initiated contemporaneously or shortly after the extensive flood basalt volcanism, although its exact timing remains controversial. The initial phases of continental rifting corresponded to the

activation of long, widely spaced and large-offset border faults, characterised by a general en-echelon arrangement Corti (2009). Boccaletti et al. (1998) also described these faults as normally long, widely spaced and characterised by large vertical offsets (>1 km). In the Northern MER, the border faults are oriented ~N40°E Corti (2009), which is consistent with horizontal gradient map produced in this study (Fig 5.2). According to Corti (2009) deformation on these faults was accompanied by progressive subsidence of the rift depression and the development of locally asymmetric basins with up to 5 km of syn-rift sediments accumulation. The southeastern rift margin in the study area is marked by the major border fault systems of Arboye and Sire which can be seen in the modeling section of Figs 6.3, 6.4, 6.5 & 6.6 which form a staircase pattern rising to > ~2600-m elevation of the uplifted rift flanks (Wolfenden et al., 2004). Seismic refraction studies in the central part of this rift sector indicate that the general form of the rift basin is asymmetric with tilting to the southeast toward the large offset Arboye normal faults and maximum thickness of the basin fill estimated to be of about 5 km (Mackenzie et al., 2005). Magnetotelluric studies Whaler and Hautot (2006) support an asymmetric structure of the basin and tilting towards the Arboye fault. Deformation continued (during Pliocene times) along large border fault systems, with slip on these faults giving rise to a deepening of the rift floor. At about 2 Ma, the deformation style changed dramatically: extension shifted from the few widely-spaced border faults with large vertical displacements, to the right-stepping arrangement of dense fault swarms with small vertical offset of the Wonji segments obliquely affecting the rift floor. This shift was concomitant with a focusing of Quaternary volcanic activity within the rift depression along the Wonji faults, giving rise to magmatic segments with only minor activity outside the en-echelon deformation belt these fault zones. (Kendall et al., 2005) the strong alteration of the lithosphere exerted by magmatic processes suggests a magmatic control on the change in deformation style from the boundary faults to the magmatic Wonji segments. The modeling result suggest that the presence of magmatic segments at Precambrian basement with the top 8 km from the surface extending to 16 km. Mahatsente et al. (1999) predict dense intrusions in both the middle and lower crust beneath the magmatic segments along the axis of the rift. The magmatic segments in the Northern MER may represent a precursor to seafloor spreading centers, developing within a lithosphere that is transitional between continental and

oceanic (Ebinger and Casey, 2001; Keranen et al., 2004; Rooney et al., 2007; Daly et al., 2008).

2. Crustal structures

The final gravity model shown in Fig 6.7 shows the root mean square error between the observed and calculated gravity values to be 2.912 mGal. The model consists of a thin ($0 - 5\ km$) near surface layer of low-density volcanic and sedimentary rocks. The basement topography observed on the eastern side of the rift as deduced from the gravity modeling in Figs 6.3, 6.4, 6.5 & 6.6 correlates with the uplifted rift flank and it is attributed to the Arboye border fault (Mackenzie et al., 2005). The deep basin (up to $5\ km$) seen in the models of Figs 6.4 & 6.5 beneath the southeastern rift flank could be a Mesozoic extensional basin which is consistent with the arguments forwarded by Korme et al. (2004) who interpret graben structures in terms of Mesozoic faulting reactivated by rift extension. In the upper crust there is a high density ($3.00\ gm/cm^3$) region between depths of 8 to $16\ km$ directly beneath the volcanic centers. The width of this body ($\sim 15 - 20\ km$) is equivalent to that of the coincident high velocity upper crustal zone identified by Keranen et al. (2004) and to that of a near coincident high conductivity anomaly identified by Whaler & Hautot (2006). The top surface of this body ($8\ km$) beneath the rift floor, is equivalent to the depth at which Keranen et al. (2004) identify the top surface of the high velocity upper crustal zone, but shallower than the depth ($15\ km$) of the conductive body reported by Whaler & Hautot (2006). The denser lower crust which has similar thickness through the profile could simply indicate a higher amount of magmatic modification of the pre-rift crust by basaltic melts. However, it may also represent the high velocity lower crust or transitional crust that is seen on some volcanic rifted continental margins (Menzies et al., 2002). In general the crust is thinner beneath the rift axis than beneath the eastern and western side of the rift zone. The upper crust is thin in the northern MER ($\sim 22 - 23$ km) as compared to the central and southern MER and thicker than southern Afar region.

CHAPTER SEVEN

CONCLUSION AND RECOMMENDATIONS

7.1 Conclusion

Based on the results obtained and the interpretations made, the analysis of gravity data of the study in the Main Ethiopian Rift has led to the following summarized conclusion.

The result of Complete Bouguer gravity analysis clearly shows an increase in gravity value towards SW to NE direction of the rift lineament whereas the residual anomaly maps reveal local subsurface structures that show a narrow zone within the NMER dominated by gravity maxima that occur at Gedemsa / Koka, Boset / Kone and Fentale magmatic segments. The result obtained from the horizontal gradient map shows the edge of the eastern rift margin (border faults).

The 2.5D models shows that the gravity field of the area were the result of the density difference between sedimentary sequence & volcanic rocks and the depth of the Moho together with the existence of magmatic segment. The sedimentary sequence are affected by a variety of faults in addition to the presence of these magmatic segments. This led to change in sedimentary thickness. The high density magmatic segments are probably related to the intrusion of molten material coming from the upper mantle into the normal fault pattern (complex of the rift). The long wavelength and maximum amplitude of the gravity field is an indicator for the presence of magmatic segments (Gedemsa, Boset and Fentale) with a top at 8 km depth extending to 16 km at the Precambrian basement. Whereas the short wave length and low amplitude gravity field shows the presence of geologic structures (contact/discontinuities). The major border fault (Arboye and Asela Sire) can be seen in the modeling section of Figs 6.3, 6.4, 6.5 & 6.6 with a depth of up to 5km. The model section of Fig 6.7 shows the crust is thinner beneath the rift axis than beneath the eastern and western side of the rift zone. The upper crust is thin in the northern MER ($\sim 22 - 23$ km) as compared to the central and southern MER and thicker than southern Afar region.

7.2 Recommendations

Based on the interpretation of the result obtained, the following recommendation are forwarded to be implemented for further analysis of subsurface geologic structures beneath both the magmatic segment and the border faults in the study area

1 Although this investigation was regional, detailed geophysical survey should be carried out at each magmatic segment and the border fault for further examination of the subsurface geological structures & there contribution to the rifting process.
2 Seismic refraction and magnetic surveys should be conducted to identify more precisely the subsurface geologic structures of the area, since these methods gives valuable information regarding to the geologic contact or discontinuities in addition to the implemented gravity method.
3 Implementation of the above recommended geophysical investigations should be integrated with other related fields of studies like structural geology for a better definition of subsurface structures.

References

Abbate E, & Sagri M. (1980) Volcanites of Ethiopian and Somali Plateaus and major tectonic lines. Atti Convegni Lincei, **47**, 219-227.

Abebe T, Manetti P, Bonini M, Corti G, Innocenti F, Mazzarini F & Pecksay Z. (2005) Geological map (scale 1:200,000) of the northern Main Ethiopian Rift and its implications for the volcano-tectonic evolution of the rift, Geological Society of America Map and Chart Series MCH094, 20 pp.

Abebe B, Acocella V, Korme T, and Ayalew D. (2007) Quaternary faulting and volcanism in the Main Ethiopian Rift. *Journal of African Earth Sciences*, **48**, 115-124.

Acocella V, Korme T, and Salvini F. (2003) Formation of normal faults along the axial zone of the Ethiopian Rift. *J. Struct. Geol.*, ***25***, 503-513.

Asfaw LM. (1990) Implication of shear deformation and earthquake distribution in the East African Rift between 4°N and 6°N. *Journal of African Earth Sciences.* **10**:745-751.

Ayele A. and Kulhanek O. (1997) Spatial and temporal variations of seismicity in the Horn of Africa from 1960 to 1993. *Geophysical Journal International,* **130**, 805–810.

Ayele, A. and Kulhanek, O. (2000) Reassessment of source parameters for three major earthquakes in East African rift system from historical seismograms and bulletins. Ann. Geofis., **43**, 81–94.

Backer BH, Mohr PA. and Williams LA. (1972) Geology of the Rift System of Africa. *Geol.Soc. Am.*, Spec. paper, 136-67.

Blakely R J, (1995) Potential Theory in Gravity and Magnetic Applications (Cambridge: Cambridge University Press).

Boccaletti M, Bonini M, Mazzuoli R, Abebe B, Piccardi L and Tortorici L. (1998) Quaternary oblique extensional tectonics in the Ethiopian Rift (Horn of Africa), Tectonophysics, **287**, 97-116.

Boccaletti M, Mazzuoli R, Bonini M, Trua T and Abebe B. (1999) Plio-Quaternary volcano tectonic activity in the northern sector of the Main Ethiopian rift: Relationships with oblique rifting: *Journal of African Earth Sciences,* **29**. 679–698.

Billham R, Bendick R, Larson K, Braun J, Tesfaye S, Mohr P and Asfaw L. (1999) Secular

and tidal strain across the Ethiopian rift, Geophysical Research Letters, **27**, 2789 2984.

Bonini M, Souriot T, Boccaletti M and Brun JP., (1997) Successive orthogonal and oblique extension episodes in a rift zone: Laboratory experiments with application to the Ethiopian rift: Tectonics,**16**, 347–363.

Bonini M, Corti G, Innocenti F, Manetti P, Mazzarini F, Abebe T and Pecskay Z. (2005) Evolution of the Main Ethiopian Rift in the frame of Afar and Kenya rifts propagation. Tectonics, 24pp.

Braile LW, Keller GR, Wendlandt RF, Morgan P and Khan MA. (1995) The East African Rift System. In: Olsen. K.H. (Ed.), Continental Rifts: Evolution, Structure, Tectonics, Developments in Geotectonics, **25**, 213-231.

Burke K and Dewey J. (1970) Plume-Generated Triple Junctions: Key Indicators in Applying Plate Tectonics to Old Rocks. *The Journal of Geology,* **81**, 406-433.

Casey M, Ebinger CJ, Keir D, Gloaguen, R. & Mohamad F. (2006) Strain accommodation in transitional rifts: extension by magma intrusion and faulting in Ethiopian rift magmatic segments. In: Yirgu G, Ebinger CJ, Maguire PKH., (Eds). (2006) The Afar Volcanic Province within the East African Rift System. Geological Society Special Publication, **259**, 143-163.

Cooper GRJ and Cowan DR (2008) Edge enhancement of potential-field data using normalized statistics *Geophysics* 73 H1–4.

Corti G.(2009) Continental rift evolution: From rift initiationto incipient break-up in the Main Ethiopian Rift, East Africa, Earth Science Reviews.

Chorowicz J. (2005) The East African Rift System. *Journal of African Earth Sciences,* **43**, 379–410.

Chorowicz J, Collet B, Bonavia F and Korme T. (1994) Northwest to North-Northwest extension direction in the Ethiopian rift deduced from the orientation of extension structures and fault-slip analysis. Geological Society America Bulletin, **105**, 1560-1570.

Cornwell DG, Mackenzie GD, England RW, Maguire PKH, Asfaw L and Oluma B. (2006): Northern main Ethiopian rift crustal structure from new high-precision gravity data. In: Yirgu G, Ebinger CJ, Maguire PKH., (Eds). (2006) The Afar Volcanic Province within the East African Rift System. Geological Society Special Publication, **259**, 307-321.

Daly E, Keir D, Ebinger C J, Stuart GW, Bastow ID and Ayele A. (2008) Crustal tomographic imaging of a transitional continental rift: the Ethiopian rift. *Geophysical Journal International*, **172**, 1033–1048.

Derek Keir PHD thesis. (2006) Strain accommodation by magmatism and faulting as rifting proceeds to breakup: Seismicity of the Northern Ethiopian Rift. Royal Holloway University of London, pp 47.

Di Paola GM. (1972): The Ethiopian Rift Valley (between 7° 00' and 8° 40' lat. North).Bull. Volcano, **36**,517-560

Dobrin MB and Savit CH. (1988): Introduction to geophysical prospecting. MCGraw. Hill Inc. Singapore.

Dugda MT, Nyblade AA, Jordi J, Langston CA, Ammon CJ and Simiyu S. (2005) Crustal structure in Ethiopia and Kenya from receiver function analysis: implications for rift development in Eastern Africa. *Journal of Geophysical Research,* 110(B1).

Dugda M, Nyblade AA and Julia J. (2007) Thin Lithosphere Beneath the Ethiopian Plateau Revealed by a Joint Inversion of Rayleigh Wave Group Velocities and Receiver Functions. *Journal of Geophysical Research,* 112pp.

Ebinger C and M Casey., (2001) Continental breakup in magmatic provinces: an Ethiopian example, *Geology*, ***29***, 527-530.

Ebinger C. (2005) Continental break-up: the East African perspective. Astronomy and Geophysics, **46**, 16-21,

Ebinger CJ, Keir D, Ayele A, Calais E, Wright TJ, Belachew M, Hammond JOS, Campbell E, and Buck WR. (2008) Capturing magma intrusion and faulting processes during continental rupture: seismicity of the Dabbahu (Afar) rift. *Geophysical Journal International,* **174**, 1138–1152.

Foster AN, Jackson JA. (1998) Source parameters of large African earthquakes: implications for crustal rheology and regional kinematics. *Geophysical Journal International,* **134**, 422-448.

Gouin P. (1979): Earthquake history of Ethiopia and the Horn of Africa. IDRC, Ottawa, 258 pp.

Gibson IL. (1969) Structural and geology of an axial portion of the main Ethiopian rift. Tectonophysics. 561-568.

Hayward N and Ebinger C. (1996) Variations in along-axis segmentation of the Afar rift system, *Tectonics*, **15**, 244-257.

Hofstetter R and Beyth M., (2003) The Afar Depression interpretation of the 1960–2000 earthquakes.*Geophysical Journal International*,**155**, 715–732.

Kazmin V and Habitemichael Berhe S., (1978) Geology and development of the Nazareth area. Ethiopian Institute of Geological Survey.

Kazmin V., (1979) Stratigraphy and correlation of volcanic rocks in Ethiopia. EIGS, note No. 106: 1-26

Kazmin V, Seife MB, Nicoletti M, and Petrucciani C., (1980) Evolution of the northern part of the Ethiopian Rift. In: Geodynamic Evolution of the Afro-Arabian Rift System, Accademia Nazionale Dei Lincei, Atti dei Convegni Lincei, **47**, 275-292.

Kebede F, and Kulhanek O. (1991) Recent seismicity of the East African Rift system and its implications. Physics of Earth Planetary Interiors, **68**, 259-273.

Kebede F, Vuan A, Mammo T, Costa G, and Panza GF., (1996) Shear wave velocity structure of Northern and North-eastern Ethiopia. Acta Geodaetica et Geophysica, **31**, 145-159.

Keir D, Kendall JM, and Ebinger C. (2005) Variations in late syn-rift melt alignment inferred from shear-wave splitting in crustal earthquakes beneath the Ethiopian rift, Geophysical Research Letters, 32pp.

Keir D, Ebinger CJ, Stuart GW, Daly E and Ayele A. (2006) Strain accommodation by magmatism and faulting as rifting proceeds to breakup: seismicity of the northern Ethiopian rift. *Journal of Geophysical Research*, 111(B5).

Keller G, Harder S, O'Reilly B, Mickus K, Tadesse K, Maguire P, and The Eagle Working Group. (2004): A preliminary analysis of crustal structure variations along the Ethiopian Rift. In: Yirgu, G. et al. (Eds.), Proceedings of the International Conference on the East African Rift System. Ethiopian Geoscience and Mineral Engineering Association, Addis Ababa, Ethiopia, 97–101 pp.

Kendall JM, Stuart GW, Ebinger CJ, Bastow ID and Keir D. (2005) Magma assisted rifting in Ethiopia. Nature, **433**, 146–148.

Kendall JM, Pilidou S, Keir D, Bastow ID, Stuart GW and Ayele A. (2006) Mantle upwellings, melt migration, and the rifting of Africa: insights from seismic anisotropy. In: Yirgu G, Ebinger CJ, Maguire PKH, (Eds). (2006) The Afar

Volcanic Province within the East African Rift System. Geological Society Special Publication, **259**, 55-72.

Keranen K, Klemperer SL, Gloaguen R and Eagle working group. (2004) Three-dimensional seismic imaging of a protoridge axis in the Main Ethiopian rift. Geology, 32, 949–952.

Keranen K, and Klemperer SL. (2008) Discontinuous and diachronous evolution of the Main Ethiopian Rift: Implications for the development of continental rifts. Earth and Planetary Science Lettters, **265**, 96-111.

Keranen K, Klemperer SL, Julia J, Lawrence JL, and Nyblade A. (2009) Low lower-crustal velocity across Ethiopia: is the Main Ethiopian Rift a narrow rift in a hot craton? Geochem. Geophys. Geosyst, 10pp.

Korme T, Chorowicz J, Collet B and Bonavia FF. (1997) Volcanic vents rooted on extension fractures and their geodynamic implications in the Ethiopian Rift, *J*. Volcanol. Geotherm. Res.***79***, 205-222.

Korme T, Acocella V, Abebe B. (2004) The role of pre-existing structures in the origin, propagation and architecture of faults in the Main Ethiopian Rift. Gondwana Research, **7**, 467–479.

Kurz T. Gloaguen R, Ebinger C, Casey M and Abebe B. (2007) Deformation distribution and type in the Main Ethiopian Rift (MER): A remote sensing study. *Journal of African Earth Sciences*, **48**, 100-114.

Lyatsky HV. (2005) The meaning of anomaly: Canadian Society of Exploration Geophysicists,**29**,no 6, 50 – 51.

Ma Zong-jin, GAO Xiang-lin and SONG Zhang-ran. (2006) *Chinese journal of geophysics*, **49**, 95-106.

Mackenzie GH, Thybo GH and Maguire P. (2005) Crustal velocity structure across the Main Ethiopian Rift: results from 2-dimenional wide-angle seismic modeling. *Geophysical Journal International*, **162**, 994–1006.

Mahatsente R, Jentzsch G, and Jahr T. (1999) Crustal structure of the Main Ethiopian Rift from gravity data: 3-dimensional modeling. Tectonophysics, **313**, 363-382.

Mahatsente R, Jentzsch G , and Jahr T. (2000) Three- dimension inversion of gravity data from the Main Ethiopian Rift. *Journal of African Earth Science*, **31**, 451-466.

Maguire PKH, Keller GR, Klemperer SL, Mackenzie GD, Keranen K, Harder S, O'Reilly B, Thybo H, Asfaw L, Khan MA, and Amha M. (2006) Crustal structure of the Northern Main Ethiopian Rift from the EAGLE controlled source survey; a snapshot of incipient lithospheric break- up. In: Yirgu G, Ebinger CJ, Maguire PKH, (Eds). (2006) The Afar Volcanic Province within the East African Rift System. Geological Society Special Publication, **259**, 269-291.

Menzies MA, Klemperer SL, Ebinger CJ & Baker J. (2002) Characteristics of volcanic rifted margins. In: Menzies MA, Klemperer SL, Ebinger CJ & Baker J. (eds) Magmatic Rifted Margins. Geological Society of America Special Paper, 362, 1–14.

Meyer W, Pilger A, Rosler A and Stets J. (1975) Tectonic evolution of the northern part of the Main Ethiopian Rift in Southern Ethiopia. In: Pilger A and Rosler A (Eds.), Afar Depression of Ethiopia, Schweizerbart, Stuttgart, 352-362.

Mickus K, Tadesse K, Keller GR and Oluma B. (2007): Gravity analysis of the main Ethiopian rift. *Journal of African Earth Sciences*, **48**, 59-69.

Miller HG and Singh V (1994) Potential field tilt-a new concept for location of potential field sources *J. Appl. Geophys,***32** 213–217.

Mohr PA. (1962a) The Geology of Ethiopia .University **college** press, Ethiopia *American Bulletin*, **102**, 439-458.

Mohr P. (1962) The Ethiopian Rift System. Bulletin of the Geophysical Observatory of Addis Ababa, **5**, 33-62.

Mohr P. (1967) The Ethiopian Rift System. Bulletin of the Geophysical Observatory of Addis Ababa, **11**, 1-65.

Mohr P. (1968) Transcurrent faulting in the Ethiopian Rift System. Nature, **218**, 938-941.

Mohr P. (1971b) Outline of tectonics of Ethiopia, UNESCO, Tectonics of Africa, **4**, 445-458 pp.

Mohr P, Mittchell JG, and Raynolds RGH., (1980): Quaternary volcanism and faulting at O'a caldera, central Ethiopian Rift. Bulletin of Volcanology, **43**, 173-189.

Mohr P. (1983): Volcano tectonic aspects of the Ethiopian Rift evolution, Bulletin Centre Recherches Elf Aquitaine Exploration Production, **7**, 175-189.

Mohr P., (1987) Patterns of faulting in the Ethiopian Rift Valley. Tectonophysics, **143**, 169-179.

Morley CK. (1999) Tectonic Evolution of the East African Rift System and its modifying influence of magmatism: A review, **2(1)**, 1-19

Nabighian MN. (1972) The analytic signal of two dimensional magnetic bodies with polygonal cross-section — Its properties and use for automated anomaly interpretation: Geophysics, **37(3)**, 507-517.

Nafe JE & Drake CL. (1957) Variation with depth in shallow and deep water marine sediments of porosity, density and the velocities of compressional and shear waves. Geophysics, **22**, 523-552.

Reid AB, Allsop JM, Granser H, Millett AJ, and Somerton IW., (1990) Magnetic interpretation in three dimensions using Euler deconvolution: Geophysics, **55**, 80–91.

Rooney T, Furman T, Yirgu G and Ayelew D. (2005) Structure of the ethiopian lithosphere: evidence from mantle Xenoliths. Geochemica et Cosmochimica Acta, **69**, 3889–3910.

Rooney T, Furman T, Bastow I, Ayalew D, and Yirgu G. (2007) Lithospheric modification during crustal extension in the Main Ethiopian Rift. *Journal of Geophysical Research*, 112pp.

Rosendahl BL. (1987) Architecture of continental rifts with special reference to east Africa: Annual Reviews of Earth and Planetary Sciences, **15**, 445-503.

Roest WR, Verhoef J, and Pilkington M. (1992) Magnetic interpretation using the 3-D analytic signal: Geophysics, **57(1)**, 116 – 125.

Rowland JR, Baker E, Ebinger C, Keir D, Kidane T, Biggs J, Hayward N and Wright T. (2007): Fault growth at a nascent slowspreading ridge: 2005 Dabbahu rifting episode, Afar.*Geophysical Journal International*, 171pp.

Soliva R, and Schultz RA. (2008) Distributed and localized faulting in extensional settings: Insight from the North Ethiopian Rift–Afar transition area. Tectonics, 27pp.

Speight J, Skelhorn R, Sloan T, and Knapp R. (1982) The dyke swarms of Scotland, in Sutherland, D.S., ed., Igneous rocks of the British Isles: London, John Wiley, 449–459 pp.

Stuart GW, Bastow ID and Ebinger CJ., (2006) Crustal structure of the northern Main Ethiopian Rift from receiver function studies. In: Yirgu G, Ebinger CJ, Maguire PKH., (Eds)., (2006) The Afar Volcanic Province within the East African Rift System. Geological Society Special Publication, **259**, 253-267.

Tiberi C, Ebinger C, Ballu V, Stuart G and Oluma B. (2005): Inverse models of gravity data from the Red Sea-Aden-East African rifts triple junction zone. Geophysical Journal International, **163**, 775–787.

Telford WM, Sheriff RE, and Geldart LP., (1990) Applied Geophysics, Second ,ed., Cambridge, Cambridge University Press, 6 – 51.

Tessema A and Fontaine LAG., (2004) Processing and interpretation of the gravity field of the East African Rift: implication for crustal extension. Tectonophysics, **394**, 87-110.

Thompson DT. (1982) EULDPH—A new technique for making computer-assisted depth estimates from magnetic data: Geophysics, **47**, 31–37.

Tiberi C, Ebinger C, Ballu V, Stuart G and Oluma B. (2005): Inverse models of gravity data from the Red Sea–Aden–East African rifts triple junction zone. *Geophysical Journal International*, **163**, 775–787.

Torge W. (1989) Gravimetry, Walter de Eruyter and Co, Berlin, Germany.

Whaler KA and Hautot S. (2006) The electrical resistivity structure of the crust beneath the northern Main Ethiopian Rift. In: Yirgu G, Ebinger CJ, Maguire PKH., (Eds)., (2006) The Afar Volcanic Province within the East African Rift System. Geological Society Special Publication, **259**, 293-305.

WoldeGabriel G, Aronson JL and Walter RC., (1990) Geology, Geochronology and Rift Basin Development in the central sector of the Main Ethiopian Rift. *Geological Society of American Bulletin*, **102**, 439-458.

WoldeGabriel G, Heiken G, White TD, Asfaw B, Hart WK, Renne PR. (2000) Volcanism, tectonism, sedimentation, and the paleoanthropological Record in the Ethiopian Rift System. In: McCoy FW, and Heiken G., (Eds.), Volcanic Hazards and Disasters in Human Antiquity. Geological Society of America Special Paper, **345**, 83-99

Wolfenden E, Ebinger C, Yirgu G, Deino A and Ayalew D. (2004) Evolution of the northern Main Ethiopian rift: birth of a triple junction, *Earth Planet. Sci. Lett.*, **224**, 213-228.

Wolfenden E, Ebinger C, Yirgu G, Renne P and Kelley SP. (2005) Evolution of the southern Red Sea rift: Birth of a magmatic margin, *Bull. Geol. Soc. Am.*, **117**, 846-864.

Wanyin W, Yu P and Zhiyun Q. (2009) A new edge recognition technology based on the normalized vertical derivative of the total horizontal derivative for potential field data *Appl. Geophys.* **6**, 226–33.

Xu Y, Hao T, Zhao B, Lihong Z, Zhang L, Li Z and Huang S. (2011): Investigation of igneous rocks in Huanghua depression, North China, from magnetic derivative methods, *J. Geophys. Eng,* **8**, 74–82.

Yemane TG, WoldeGebriel G, Tesfaye S, Derhe SM, Durary S, Ebinger C, and Kelley S. (1999): Temporal and Geochemical characteristics of Tertiary volcanic rocks and tectonic history in the southern MER and the adjacent volcanic field. Acta, **2(1)**, 99-119

Declaration

I declare that this thesis is my original work carried out under the supervision of Dr. Tilahun Mammo, has not been presented for degrees in any other University and all Sources of material used for the thesis have been duly acknowledged.

Name: Fithat Habteweld Kassa

Signature: _____

Date: _____

This thesis has been submitted for examination with my approval as a University advisor

_____

Dr. Tilahun Mammo